Avinashilingam Institute for Home Science and Higher Education for Women
Deemed to be University Estd.u/s 3 of UGC Act 1956, Category A by MHRD
Re-accredited with 'A^{++}' Grade by NAAC.CCPA 3.65/4, Category I by UGC
Coimbatore-641043, Tamil Nadu, India

Coagulation Proteins in Rats during Hypoxia Reversal by Oxygen Nanobubbles

By

Akalya Bai. S. K

21PBC002

II M.Sc. Biochemistry

Department of Biochemistry, Biotechnology and Bioinformatics

A thesis submitted to Avinashilingam Institute for Home Science and Higher Education for Women, Coimbatore - 641043

In partial fulfilment of the requirement for the degree of
MASTER OF SCIENCE IN BIOCHEMISTRY

MAY 2023

CERTIFICATE

Coagulation Proteins in Rats during Hypoxia Reversal by Oxygen Nanobubbles

By

Akalya Bai. S. K

21PBC002

II M.Sc. BIOCHEMISTRY

A thesis submitted to Avinashilingam Institute for Home Science and Higher Education for Women, Coimbatore - 641 043.

In partial fulfilment of the requirement for the degree of MASTER OF SCIENCE IN BIOCHEMISTRY

MAY 2023

Signature of the Supervisor

17/5/2023

Signature of Head of the Department

ACKNOWLEGEMENT

ACKNOWLEDGEMENT

I owe a special tribute to **God Almighty** for the opportunity given to take up to complete my work successfully. In addition to the will of supreme divinity, the willingness of many subject experts and erudite scholars to extend their assistance and help for completion of a work plays an important role.

I express my deep sense of gratitude to all the higher authorities of Avinashilingam Institute for Home Science and Higher Education for Women, Coimbatore for their immense support.

I take the opportunity to express my sincere thanks to **Dr. Prof. S.P. Thiyagarajan**, Chancellor, Avinashilingam Institute for Home Science for Higher Education for Women, Coimbatore, for providing the opportunity and infrastructure to undertake this investigation.

I immensely thank **Dr. V. Bharathi Harishankar**, Vice Chancellor, Avinashilingam Institute for Home Science and Higher Education for Women, Coimbatore, for providing the entire facilities essential to carry out and complete the study.

I record my sincere thanks to **Dr. S. Kowsalya**, Registrar, Avinashilingam Institute for Higher Education for Women, Coimbatore, for timely help rendered to carry out the work.

I express my special gratitude to **Dr. A. Vijayalakshmi**, Dean, School of Biosciences, Avinashilingam Institute for Home Science and Higher Education for Women, Coimbatore, for providing the opportunity and timely help rendered to carry the work successfully.

I express my reverential thanks to **Dr. P. Lalitha**, Director, Research and Consultancy, Avinashilingam Institute for Home and Higher Education for Women, Coimbatore for her support and encouragement rendered towards the completion of my thesis work.

I record my sincere gratitude to **Dr. Anitha Subash**, Professor and Head, Department of Biochemistry, biotechnology and Bioinformatics, Avinashilingam Institute for Home Science and Higher Education for Women, Coimbatore, for her immense support and motivation throughout my study.

I owe my indebtedness, profound and deepest thanks to my guide **Dr. E. Nithya**, Assistant Professor, Department of Biochemistry, Biotechnology and Bioinformatics, Avinashilingam Institute for Home Science and Higher Education for Women, Coimbatore, for her incessant guidance, immense tolerance, meticulous care, good support, creative influences, thoughtful advice, steady encouragement, motherly love throughout the research and motivation right from selection of topic to the completion of the work effectively and efficiently.

I am indebted to **Dr. S. Velvizhi** for her invaluable help rendered throughout the study period.

I extend my sincere gratitude to **Avinashilingam University**, for granting funds for the project through Seed Money Project.

I submit my sincere thanks to all The Staff Members of Department of Biochemistry, Biotechnology and Bioinformatics, Avinashilingam Institute for Home Science and Higher Education for Women, Coimbatore, for lending their helping hand and invaluable guidance during the course of this thesis work.

I place my gratitude to the feet of my parents for their immense support and guidance during the course of my study.

I express my sincere heartfelt thanks to my friends at the Department of Biochemistry, Biotechnology and Bioinformatics, for giving affectionate advice, unconditional love and incredible support for completion of my project work.

I acknowledge the contribution of all other unseen hands during the course of the study for help rendered in successful completion of the study.

AKALYA BAI. S. K

CONTENTS

CONTENTS

LIST OF TABLES

LIST OF FIGURES

LIST OF APPENDICES

1.0 INTRODUCTION

Earth's climate changed when cyanobacteria that produce O_2 and use water as a terminal reductant appeared. This made the planet more favorable to the development of aerobic metabolism and complicated life. The invention of water oxidation enabled photosynthesis to colonize new habitats, drastically modifying the Earth's surface (Baracaldo *et al*., 2020).

Photosynthesis is responsible for almost all of the natural oxygen in the atmosphere. Green plants use the sun's energy to assimilate carbon dioxide and create free oxygen, whereas animals and some microbes use the atmosphere's oxygen during respiration to create carbon dioxide. At 20°C (68 °F), 100 parts of pure water dissolve approximately 3 parts of oxygen by volume; in saltwater, the amount dissolves slightly less. For fish and other aquatic species to breathe, dissolved oxygen is required (Stirbet *et al*., 2020).

Since oxygen keeps life on Earth alive, it is necessary for all living things. It is said that oxygen is required for 90% of our body's biological and physiological processes. Our cells are fuelled by oxygen, which also serves to supply the fundamental building elements required for survival. In order to create proteins that help our cells divide, our cells combine oxygen with nitrogen and hydrogen. Carbohydrates, which give our cells the energy they need to function are produced when oxygen is joined with carbon and hydrogen. Oxygen is also necessary for constructing replacement cells for our bodies. About 700 billion of our body's cells need to be changed every day due to wear and tear. These new cells cannot be produced by our bodies without air.

Cellular respiration is the process by which organisms combine oxygen with food molecules, converting the chemical energy in these substances into life-sustaining molecules and discarding them as waste products, carbon dioxide and water. The quantity of oxygen in the tissues must change in response to a gradient of pressure that forces oxygen into the tissues through membrane diffusion in order to sustain homeostasis (Zenewicz, 2017). Hypoxia is a situation where the body or a specific area of the body does not receive enough oxygen at the cellular level (Maclntyre. 2014).

Hypoxia can be categorized as either generalized (affecting the entire body) or localized (affecting a specific area of the body) (Das *et al*., 2019). Hypoxia is distinct from hypoxemia and anoxemia in that it pertains to a condition where there is inadequate oxygen in a tissue or throughout the body, whereas hypoxemia and anoxemia are conditions where there is little to no oxygen in the blood (Maclntyre. 2014). Anoxia is a type of hypoxia in which there is no oxygen flow at all.

Hypoxia can occur due to external or internal causes. When the breathing gas is hypoxic, hypoxia can result from external causes. Internal causes are decreased lung gas exchange efficiency, decreased blood oxygen carrying capacity, impaired general or local perfusion, or the inability of the affected tissues to extract oxygen from RBCs or metabolically process an adequate supply of oxygen from an adequately oxygenated blood supply. Low oxygen amounts in the bodily tissues results in hypoxia. It results in symptoms like bluish skin, confusion, restlessness, difficulty breathing, and a fast heart rate. People may be at risk for hypoxia if they have one of many chronic cardiac and respiratory problems. Having hypoxia can be fatal (Varney *et al*., 2022).

There is a critical level of oxygen delivery (DO_2) below which tissue oxygen consumption drops and becomes dependent on DO_2, leading to tissue hypoxia. The various mechanisms of tissue hypoxia include circulatory, anemic and hypoxic factors, each of which is characterized by a reduced level of oxygen delivery (DO_2) but a conserved ability to increase oxygen extraction. Another form of tissue hypoxia caused by a deficiency in mitochondrial respiration, known as cytopathic hypoxia, can be seen in septic situations with normal overall DO_2. With increased stopped-flow capillaries, decreased functional capillary density and marked heterogeneity between areas with large intercapillary distance, sepsis alters the microcirculation, impairing the ability of the tissue to extract oxygen and to meet the elevated tissue oxygen demand, which results in the development of tissue hypoxia (Mallat *et al*., 2022).

Hypoxia has critical roles in cancer development, progression, and metastasis. Since the blood supply for the rapidly expanding tumour cells quickly becomes insufficient, hypoxia is primarily seen in tumour environments. By controlling the expression of genes involved in angiogenesis, glycolytic metabolism and other biological processes, hypoxia activates HIF-1 to

promote carcinogenesis and tumour growth. When the tumour suppressor protein, pVHL, has been hydroxylated under normoxic conditions, HIF-1 binds to it and triggers its proteasomal destruction. A number of oncogenes are activated as a result of the HIF-1 heterodimer stabilizing and moving into the nucleus during hypoxia. The hypoxic control of oncogenes by pVHL provides insight into cancer pathogenesis (Yeo, 2019).

Acute hypoxemia, post-operative situations, pneumothorax and irregularities in the quality and quantity of hemoglobin are the most frequent causes for initiating oxygen therapy. Raising the head of the bed increases inhalation, encourages diaphragmatic descent and lessens the work required for breathing. In all hypoxic persons, positioning improves airway patency. Patients can successfully clean their airways while preserving their oxygen levels by using deep breathing and coughing strategies. In hyperbaric oxygen therapy, patients receive 100% oxygen at pressures above atmospheric pressure to address illnesses that are caused by hypoxia and inflammation (Liu *et al*., 2021).

Traditionally, hypoxia management involves attempts to increase oxygen supply, with an emphasis on blood oxygenation (PO_2 and Hb) and cardiac output. Positive-pressure breathing and additional oxygen are frequently used to increase PO_2, which exposes patients to the risks of oxygen toxicity and ventilator-induced lung damage. Patients receiving transfusions are at risk for immunologic problems, fluid excess and potentially serious pulmonary damage. Patients are at risk for fluid overflow and extra adrenergic activation when their cardiac output is increased. Consequently, increasing the physiology of oxygen distribution, like so many other treatments used in critical care, may not transfer into better results and must always be applied carefully (Maclntyre, 2014).

Controlling oxygen intake is an additional strategy for influencing cellular oxygenation. Globally, this can be accomplished by controlling pain, fever, anxiety, neuromuscular inhibition, or chilling (eg., therapeutic hypothermia after cardiac arrest) (Burtscher *et al*., 2021). To different degrees, each of these can reduce O_2 requirements in particular tissue layers to enhance local tissue oxygenation. These tactics may, however, be poisonous in and of themselves. Narcotics and anxiety medications, for instance, can extend the need for artificial ventilation (Jackson *et al*.,

2015), and neuromuscular inhibition can cause respiratory muscle atrophy from lack of use (Lewis *et al*., 2016).

Nanotechnology has been a known field of research since last century. Since ‘‘nanotechnology” was presented by Nobel laureate Richard P. Feynman during his famous 1959 lecture ‘‘There’s Plenty of Room at the Bottom”, various revolutionary developments have occurred in the field of nanotechnology. In recent years, nanotechnological techniques have been introduced in a wide range of sectors to provide a more efficient and effective option for fixing an issue or providing a superior product.

It is important to distinguish between nanotechnology and nanoscience. Nanotechnology is the ability to see, measure, manipulate, assemble, control and construct matter at the nanoscale scale. Nanoscience is a convergence of physics, materials science and biology, which deals with manipulation of materials at the atomic and molecular dimensions (Bayda *et al*., 2019).

The development of nanoscience and nanotechnology has impacted various scientific fields in a variety of ways. For example, in physics, different microscopes are now able to observe objects at scales ranging from micro to nano. In chemistry, carbon dots can be seen at scales ranging from micro to nano. In computer science, room-sized computers have been replaced by portable, thin laptops. And in biology, single complex biomolecules can be studied at the nano level (Bayda *et al*., 2019). Nanotechnology and nanoscience have quickly risen to the top of the list of requirements for both commercial and medical applications, including imaging probes, drug delivery systems and diagnostic biosensors (Hulla *et al*., 2015).

Nano-materials are usually considered as substances with one or more exterior dimensions between one and one hundred nanometres (Hulla *et al*., 2015). Nanomaterials have advanced quickly in the past ten years and opened up new avenues in biomedical uses for drug delivery, imaging and different tumor therapeutic methods such as photothermal therapy, radio-sensitization therapy, magnetic therapy and photo dynamic therapy (Sun *et al*., 2020; Li *et al*., 2018 & Adeel *et al*., 2020).

Novel bio nanotechnology employing engineered micro and nano structures have been developed for diagnostic and therapeutic applications in the field of healthcare. Nanovesicles, nanodroplets and nanobubbles have been examined as a substitute to readily available ultrasound contrast agents (Hadinger *et al*., 2018, Rojas *et al*., 2019, Nyankima *et al*., 2018, Xie *et al*., 2018 & Dong *et al*., 2019).

Micro and nanobubbles are one of those new assemblies already in use in a variety of medical applications (Khan *et al*., 2018). Micro/nanobubbles (MNBs) are spherical vesicles with an enclosed shell and a centre that have been used as ultrasonic contrast agents in medicine for several decades (Kheir *et al*., 2012 & Khan *et al*., 2018). Due to their micrometer size, ultrasonic contrast agents are frequently referred to as "microbubbles" (Cavalli *et al*., 2016). A non-invasive real-time molecular imaging method called photoacoustic imaging, which is based on the optical absorbance of tissues, has also used microbubble-based contrast agents (Huynh *et al*., 2014, Wilson *et al*., 2013 & Dixon *et al*., 2015). Nanobubbles are a new generation of responsive nanocarriers with the goal of increasing *in vivo* performance.

Due to their nanometer dimension, nanobubbles have been studied for diagnostic and medicinal reasons in order to increase cellular penetration (Bhandari *et al*., 2017, Cavalli *et al*.,2013, Cavalli *et al*., 2016 & Zhou *et al*., 2012). These nanobubbles were initially intended to be contrast agents (Cavalli *et al*., 2016), and when exposed to sonic fields, they produced asymmetric oscillations in diameter. The use of nanobubbles as ultrasound contrast agents for tumour imaging and drug/gene delivery uses has also been studied by a number of other researchers (Zhou *et al*., 2012, Fix *et al*., 2015 & Wu *et al*., 2013). It is remarkable that nanoscale bubbles enable extravasation from blood arteries into adjacent tissues, increasing delivery effectiveness and localization (Cavalli *et al*., 2013). Both the enhanced permeability and retention effect (Fang *et al*., 2011) and active targeting, or antibodies attaching to the bubble surface (Fokong *et al*., 2012 & Zhang *et al*., 2013), may cause them to assemble within tumor tissues.

Nanobubbles have monolayer shells surrounding a hydrophobic gas core, making them suitable for gas delivery uses. In contrast to nanosized liposomes, which have a lipid bilayer membrane and hydrophilic aqueous center, nanobubbles have monolayer shells (Khan *et al*., 2018,

Bhandari *et al*., 2017 & Koshiyama *et al*., 2016). For oxygen distribution, both nano and micro-sized bubbles have been used (Kheir *et al*., 2013). Nanobubbles are potential for gas and medication delivery uses due to their increased surface contact area, smaller size, polydisperse size distribution, greater payload, higher cellular uptake and an effective gas delivery mechanism (Yoon *et al*., 2014).

As the gaseous molecules mediate numerous cells signaling pathways and play crucial physiological roles and have been shown to elicit biological responses, the administration of therapeutic gases like nitric oxide, hydrogen sulphide, carbon monoxide and oxygen is gaining more attention (Fix *et al*., 2015). Since many medical conditions, including diabetes, burns, bedsores and other wounds, are linked to inadequate oxygen supply to tissues, oxygen delivery is particularly interesting (Cavalli *et al*., 2016). The use of nanobubbles that are directly or indirectly responsive to ultrasound has been suggested as a possible method for delivering oxygen. The ultrasound-direct-responsive nanobubbles exhibit good safety oxygen storage and encapsulation capacity (Cavalli *et al*., 2009).

The present study aims to assess whether nanobubbles containing oxygen as core gas have the potential to reverse acute hypoxia in the animal model rats.

2.0 REVIEW OF LITERATURE

The Review of Literature pertaining to the study entitled “Coagulation Proteins in Rats during Hypoxia Reversal by Oxygen Nanobubbles” is discussed under the following headings:

2.1 Oxygen

2.1.1 Evolution of Oxygen

2.1.2 Oxygen in Humans

2.2 Hypoxia

2.2.1 Causes of Hypoxia

2.2.1.1 Hypoxemia

2.2.1.2 Impaired Oxygen Transport to Tissues

2.2.1.3 Impaired Oxygen Extraction/Utilization

2.2.2 Types of Hypoxia

2.2.2.1 Hypoxemic Hypoxia

2.2.2.2 Anemic Hypoxia

2.2.2.3 Circulatory Hypoxia

2.2.2.4 Histotoxic Hypoxia

2.2.3 Compensatory Mechanisms

2.2.3.1 Polycythaemia

2.2.3.2 Hypoxia Inducible Factors

2.2.4 Hypoxia in Tumors

2.2.5 Treatment of Hypoxia

2.2.5.1 Hyperbaric Oxygen Therapy

2.2.5.2 Non-Invasive Ventilation

2.2.5.3 Continuous Positive Airway Pressure

2.2.5.4 High-Flow Nasal Cannula Therapy

2.3 Nanotechnology

2.3.1 Nanomedicine

2.3.2 Nanocarriers

2.3.2.1 Oxygen Carrying Strategies

2.3.2.1.1 Nanobubbles

2.3.2.1.2 Artificial Red Blood Cells

2.3.2.1.3 Perfluorocarbons

2.3.2.1.4 Nanoscale metal-organic frameworks

2.4 Nanobubbles

2.4.1 Shell Types

2.4.1.1 Lipid Shells

2.4.1.2 Protein Shells

2.4.1.3 Polymer Shells

2.4.2 Characterisation Techniques

2.4.3 Synthesis of Nanobubbles

2.4.3.1 Ink Jet Method

2.4.3.2 Laser Ablation Method

2.4.3.3 Emulsification Method

2.4.3.4 Agitation Method

2.4.3.5 Microfluidic Method

2.4.3.6 Sonication Method

2.4.4 Application of Nanobubbles

2.4.4.1 Biomedical Imaging

2.4.4.1.1 Ultrasound Contrast Enhancement

2.4.4.1.2 Photoacoustic Contrast Enhancement

2.4.4.1.3 Molecular Imaging

2.4.4.2 Dentistry

2.4.4.4 Gene Delivery

2.4.4.4.1 Plasmid DNA Delivery

2.4.4.4.2 Oligonucleotide Delivery

2.4.4.5 Tumor Ablation

2.4.4.5 Oxygen Delivery

2.4.4.3.1 Wound Healing

2.4.4.3.2 Tumor Hypoxia Treatment

2.1 Oxygen

The chemical element oxygen is a non-metallic, colorless and odorless element that belongs to group 16 of the periodic table. Carl Wilhelm Scheele, a Swedish scientist, discovered it around 1772 by heating potassium nitrate, mercuric oxide and other substances. It comes in diatomic (O_2) and triatomic allotropic types (O_3, ozone). The paramagnetism of oxygen is explained by the diatomic form's characteristics, which suggest that six electrons bind the atoms and two electrons are left unpaired. The ozone molecule's three elements are not arranged in a linear line.

2.1.1 Evolution of Oxygen

Photosynthesis serves as the most important worldwide mechanism for replenishing atmospheric and marine oxygen, which is required to support all aerobic life. According to geochemical records of land oxides, O_2 evolution must have occurred in the cyanobacteria's forerunners before ca. 2.8 billion years ago and resulted in the buildup of O_2 in the atmosphere. The crucial step in the development of life on Earth was the formation of a photosynthesis device that could divide water into oxygen, protons and electrons. By using water as a reductant, photosynthesis now has an infinite supply of electrons and protons. By liberating photosynthesis from the constraints imposed by the abundance of reduced chemical substances, the world output of organic carbon could be massively expanded, opening up new environments for photosynthesis to occur. The Earth's surface was physically altered by this occurrence. The development of aerobic breathing, which uses a more potent metabolic energy source, was a result of the buildup of O_2 in the environment. Because aerobic metabolism produces 18 times more energy (ATP) per metabolic intake (hexose sugar) than anaerobic metabolism, the engine of life became supercharged. Eukaryotic creatures, which are complicated, multicellular and energy-efficient, emerged as a result of these evolutionary stages (Willhite *et al*., 2014).

2.1.2 Oxygen in Humans

In humans, oxygen is inhaled through lungs at the same time carbon dioxide leaves the circulation and enters the alveoli during breathing. The trachea, bronchial passages, nostrils and mouth are ultimately used to guide this carbon dioxide out of the human body for exhalation. Following that, the human circulation system distributes oxygen throughout the body and returns

carbon dioxide to the lungs. Every time a person breathes, the complete procedure is repeated. This process of delivering oxygen to tissues is known as perfusion (Chris *et al*., 2019).

To satisfy daily energy needs, humans use oxygen to obtain about 2550 calories from food. A daily requirement of 22 molecules of dioxygen, or 2.5×10^{-4} mol s^{-1}, is needed for this combustion. This represents an average oxygen utilization rate of 2.5×10^{-18} mol/cell per second. Depending on the sort of cell, its purpose and its biological state, cells can utilize oxygen in a variety of ways. Mammalian cells *in vitro* have been observed to use oxygen at rates as high as 350 amol cells per second (Petersson *et al*., 2014).

2.2 Hypoxia

Hypoxia is a condition in which the cell has a reduced oxygen level and partial pressure. A cell's response to different levels of hypoxia can vary from significant adaptation to cell death depending on the type of cell, its metabolic requirements and its capacity to adjust to hypoxia. Individual tissues have differing oxygen tensions and oxygen demands; on average, tissues at rest utilize 5–6 mL of O_2 per decilitre of blood delivered. Hypoxia could be fairly defined as a scenario when tissue fails to receive this amount of oxygen (Choudhury *et al.*, 2018).

2.2.1 Causes of Hypoxia

Hypoxemia, impaired oxygen transport to tissues and impaired tissue oxygen extraction/utilization are the three basic abnormalities that can lead to tissue hypoxia.

2.2.1.1 Hypoxemia

Hypoxemia is a below-normal level of oxygen in the blood, especially in the arteries. When a person cannot breathe at normal rate, alveolar CO_2 rises while the (partial oxygen pressure) PaO_2 decreases to a similar extent as the (partial pressure of carbon-di-oxide) $PaCO_2$. The alveolar-arterial gradient (A-a gradient) fails to increase as a result of these opposing and about equal changes. If a patient has hypoventilation, associated diffusion impairment, ventilation/perfusion (V/Q) mismatch, or right-to-left shunting, the A-a gradient will increase in that patient. Centrally acting respiratory depressants, neuromuscular conditions that impair breathing muscles, chest wall

injuries, pleural space lesions and upper airway blockage are all causes of hypoventilation (Bach, 2017).

2.2.1.2 Impaired Oxygen Transport to Tissues

The process of transporting oxygenated blood from the alveolar capillaries to the organs is known as oxygen distribution. O_2 concentration and cardiac production are two variables that affect the supply of oxygen. A typical tissue oxygen supply rate of 1000 mL/min is achieved with a normal cardiac output of 5 L/min and 200 mL of O_2/L of blood. Importantly, the capacity to deliver O_2 to tissues at 5 – 7 L/min can be achieved both under exercise circumstances and in disease states (such as sepsis, thyroid storm) (Klocke *et al*., 2023).

Diffusion impairment exists when there is insufficient equilibration of O_2 tension throughout the alveoli and capillaries. O_2 quickly diffuses from the alveoli into the capillaries in healthy people. Diffusion impairment can appear earlier than V/Q mismatch in the progression of lung illness. Thickening of the capillary wall or the alveolar interstitial space impairs diffusion. The progression of this illness leads to diseases like emphysema, vasculitis, fibrosis and interstitial edema (Boysen *et al*., 2013).

2.2.1.3 Oxygen Extraction/Utilization

The process of transferring oxygen from the Hemoglobin (Hb) molecule into cells' cytoplasm and eventually into their mitochondria, where it is used for oxidative respiration, is known as oxygen extraction or utilization. Hb-O_2 affinity is affected by the early dissociation of O_2 from Hb in this process. After that, the mechanism is primarily diffusive with a significant PO_2 difference between capillary blood and mitochondria. Due to this, mitochondrial PO_2 is typically < 10 mm Hg. Only 25% of the delivered oxygen truly departs the blood and reaches the tissues at rest in the typical tissue capillary bed (extraction ratio) (Mairbarul *et al*., 2012). Accordingly, the cells absorb 250 mL of every 1,000 mL of oxygen supplied per minute, leaving 750 mL in the blood. Therefore, mixed venous oxygen saturation is at 75% and typical oxygen intake is 250 mL/min at rest, which corresponds to a mixed venous PO_2 of 40 mm Hg. In elite athletes, extraction during exertion can rise to up to 60% or 75%, leading to extremely low mixed venous oxygen contents. In the same way that blood flow and oxygen distribution vary by tissue, so does oxygen

absorption. Disruptions in oxygen utilization by the mitochondria and tissue extraction are linked to a variety of inflammatory illness conditions (such as sepsis) (Maclntyre, 2014). Poisons like cyanide may hinder the mitochondria's ability to use oxygen (Hamel *et al*., 2011). Under these conditions, mixed venous oxygen concentrations are often high.

2.2.2 Types of Hypoxia

The following things are necessary in order for oxygen to reach the cells in the tissues. air with sufficient oxygen for breathing: 1) A healthy respiratory system to deliver oxygen to the alveoli. 2) Circulatory and cardiac functioning are necessary for delivering oxygen-rich blood to the tissues. 3) Sufficient red blood cells to carry oxygen. 4) Tissue cells having the ability to use oxygen. Each of the four forms of hypoxia is brought on by a deficiency of oxygen in one of these regions.

2.2.2.1 Hypoxemic Hypoxia

Hypoxemic hypoxia is a lack of oxygen caused by low arterial blood oxygen tension as a result of the lungs' failure to adequately oxygenate the blood. Hypoventilation, reduced lung diffusion and pulmonary shunting are some of the causes (Bhutta *et al*., 2022). This is also caused by lung and cardiac illness, congenital heart defects and medicines that impede respiration. Hypoxemia can also result from traveling to a high height, where oxygen concentrations are reduced (Bach, 2017).

2.2.2.2 Anemic Hypoxia

When there aren't enough red blood cells to transport oxygen from lungs to other organs, anemic hypoxia occurs. If the body does not produce enough or produces red blood cells that are deformed, a person may become anemic. The organs receive less air as a result. Either anemia or carbon monoxide toxicity can cause such hypoxia, which prevents hemoglobin from carrying oxygen by combining with it to create carboxyhemoglobin ($HbCO_2$) (Manninen *et al*., 2016).

2.2.2.3 Circulatory Hypoxia

Circulatory hypoxia, also known as stagnant hypoxia or ischemic hypoxia, is a condition where there is insufficient blood flow, which reduces the amount of oxygen that is available to the

tissues. This condition can occur during shock, cardiac arrest, severe congestive heart failure, or abdominal compartment syndrome, where the cardiovascular system is the primary dysfunction, resulting in a significant decrease in perfusion. This could happen just in that region or all over the body. Although the lungs sufficiently oxygenate arterial gas and the tissues can utilize the available oxygen, the oxygen flow rate to the tissues is inadequate (Manninen *et al*., 2016).

2.2.2.4 Histotoxic Hypoxia

Histotoxic hypoxia is also known as cellular hypoxia or dysoxia. Although the oxygen flow is completely normal in this situation, the tissues' ability to utilize oxygen is reduced because the tissue cells are poisoned and unable to do so (Manninen *et al*., 2016). Examples include cyanide toxicity, which prevents the cytochrome C oxidase enzyme needed by mitochondria for cellular metabolism. Similar results are obtained from methanol poisoning because formic acid, which is produced during methanol metabolism, blocks mitochondrial cytochrome oxidase (Pittman, 2011).

2.2.3 Compensatory Mechanisms

When a normal process is disrupted due to disturbances, our body develops new compensatory actions to meet the normal process. In acute hypoxic conditions, the human system has some certain mechanisms to compensate for normal functioning, such as, increased production of red blood cells in and production of hypoxia inducible factors to increase the anaerobic metabolism (Maclntyre, 2014).

2.2.3.1 Polycythaemia

Polycythaemia is an increase in red blood cells in the body. If tissue hypoxia occurs, global compensatory respiratory and cardiac mechanisms similar to those seen with exercise occur to improve oxygen delivery. Clearly, these include improvements in cardiac output, hyperventilation to improve PaO_2, acidosis-related right shifting of the oxy-hemoglobin dissociation curve to enable O_2 unloading and regional pulmonary vasoconstriction to improve V/Q matching (ventilation / perfusion ratio) (Bach, 2017). But polycythaemia develops over time in both individuals at high altitude and in patients with persistent hypoxemia due to a rise in red blood cell production. Importantly, polycythaemia can thicken blood, which could possibly reduce blood flow and the vessels' ability to transport oxygen to tissues (Maclntyre, 2014).

2.2.3.2 Hypoxia Inducible Factors

In reaction to hypoxia, a collection of heterodimeric proteins known as hypoxia-inducible factors (HIFs) interact with hundreds of genes at the cellular level (Pugh, 2016 & Semenza *et al*., 2012). HIF activation causes upregulation of erythropoietin, angiogenic factors and vasoactive mediators as well as the activation of glycolytic enzymes, which results in anaerobic metabolism and the production of lactate. It also causes a mitochondrial phenomenon similar to hibernation, which lowers oxygen requirements. In reaction to hypoxia, HIFs can also suppress the activity of additional processes (Maclntyre, 2014).

2.2.4 Hypoxia in Tumors

A defining feature of the majority of advanced solid tumors is aggressive growth of cancer cells and the abnormal vascular system in the tumor region causing tumor hypoxia. Although the oxygen levels in various kinds of human tumors vary widely, the oxygen levels in tumor cells are typically much lower than those in the normal tissue around it. Hypoxia has been shown to play significant roles in chemo and radioresistance, as well as to adversely affect various anticancer treatments and encourage tumor metastasis (Sun *et al*., 2020). HIF plays a largely negative role in the regulation of immune responses inside tumors. It appears that therapeutic strategies targeting HIF in the immune system could be beneficial for anti-tumour immune responses (Kumar *et al*., 2014).

Among all malignancies, Hepatocellular carcinoma is the most hypoxic. Normal human liver tissue has a median partial pressure of oxygen (pO2) of 30 mmHg, but the intratumoral zone of human liver tumors has a pO2 of only 6 mmHg. Hypoxia induces a series of alterations of metabolic pathways via HIFs that promotes drug resistance, leading to unsatisfactory clinical outcomes in hepatocellular carcinoma patients (Bao *et al*., 2021).

2.2.5 Treatment of Hypoxia

The source of the hypoxia will determine the course of treatment. Treatment options may be confined to offer support and getting the system back to normal oxygenation, if it is found that there is an external source and it can be eliminated. In other situations, a lengthier course of therapy might be required, which might call for additional oxygen to be given continuously or for an

extended period of time. Lowering metabolic rate by lowering body temperature reduces oxygen demand and usage and helps reduce the impacts of tissue hypoxia, particularly in the brain and therapeutic hypothermia based on this concept may be beneficial (Bhutta *et al*., 2022).

2.2.5.1 Hyperbaric Oxygen Therapy

Hyperbaric Oxygen Therapy (HBOT) is the use of oxygen "as a drug to treat basic disease processes and their diseases" while under pressure. HBOT provides two to three times more oxygen than regular air pressure is delivered in a pressurized chamber, which aids in the lungs' ability to take in and utilize more oxygen.The physiologic impact of hyperbaric oxygen treatment changes the concentration of oxygen in the plasma and helps hemoglobin reach its maximum oxygen-carrying capacity. The impacts of hyperbaric oxygen change how DNA is mutated, the cell's organelles change, tissue structure is better and organ function is improved. Within 25 to 35 sessions, these alterations can become long-lasting. Every day, HBOT is presently given in chambers of various capacities, from individual rooms to operating rooms. Due to its capacity to reduce oxygen deficits, promote healing and angiogenesis, fight infection and manage inflammation, HBOT has a wide range of contemporary uses for therapy (Bhutta *et al*., 2022).

2.2.5.2 Non-Invasive Ventilation

Non-Invasive ventilation (NIV) with bilevel positive airway pressure is a non-invasive approach that refers to providing ventilatory support through the patient's upper airway using a mask or similar device. Hypoventilation can be successfully treated with this method. It is now well recognized as the recommended course of care for individuals with hypercapnic respiratory failure (HRF). NIV has been utilized in critical care units since the 1980s and after early anecdotal reports and bigger series, a number of randomized trials have been carried out well. Data from these trials have demonstrated that NIV is an effective therapy for HRF (Comellini *et al*., 2019).

2.2.5.3 Continuous Positive Airway Pressure

Continuous positive airway pressure (CPAP) is used to keep the airways open in persons who are able to breathe on their own to maintain a constant pressure in the airways. The pressure in the alveoli above atmospheric pressure at the conclusion of expiration is known as positive end-expiratory pressure (PEEP). The use of CPAP allows for the delivery of PEEP while also

maintaining the desired pressure during the whole breathing cycle, including inspiration and expiration (Gupta *et al*., 2016). Centimeters of water pressure (cm H_2O) are used to measure it. Bilevel positive airway pressure, as contrast to CPAP, delivers a different amount of pressure depending on whether the patient is breathing or exhaling (Pinto *et al*., 2022).

2.2.5.4 High-Flow Nasal Cannula Therapy

Early in the new millennium, high-flow nasal cannula (HFNC) oxygen treatment was initially used in clinical settings to treat apnea in preterm newborns as an alternative to CPAP (Nolasco *et al*., 2022). Since then, its application to children and infants with respiratory failure has progressively increased. A number of factors, such as the availability of simple-to-use devices that are remarkably well tolerated by the majority of patients when compared to CPAP or other forms of noninvasive ventilation (NIV), have led to the fact that HFNC is currently an incredibly popular form of respiratory support in pediatric care (Mikalsen *et al*., 2016). Research has been conducted to use HFNC in adults and they are turning out to be positive. The HFNC device is made to provide heated and humidified gasses, typically oxygen- and air-mixed air, at various flow rates and customizable concentrations.

2.3 Nanotechnology

Nanotechnology is the application of science, engineering and technology at the nanoscale, or between 1 and 100 nanometers. Nanoscience and nanotechnology are the study and application of extremely small things and can be used across all the other science fields, such as chemistry, biology, physics, materials science and engineering (Bayda *et al*., 2019).

2.3.1 Nanomedicine

The application of nanotechnology in the health care sector is known as nanomedicine (Viseu, 2020). Nanomaterials, biological devices, nano electronic biosensors and even potential future uses of molecular nanotechnology, like biological robots, are all included in the field of nanomedicine.

Nanomaterials have also advanced quickly in the last decade and opened up new avenues in biomedical applications for imaging, drug delivery and various tumor therapeutic modalities,

such as photothermal therapy (PTT), radio-sensitization therapy, magnetic therapy and also Photodynamic therapy (PDT) (Sun *et al*., 2020, Li *et al*., 2018 & Adeel *et al* 2020). The methods for delivering nanomedicine to the precise location of the target also stop drugs or other delivering molecules from leaking, reducing their non-specific accumulation in healthy tissues.

2.3.2 Nanocarriers

Nanocarriers are sub-micrometric particles with a size of less than 100 nm that are created with the purpose of transporting, dispersing and releasing molecules having biological activity. These nanotechnology-based drug delivery systems are regarded as effective methods for overcoming technical, biological and biopharmaceutical constraints. One of their benefits is the potential to create multifunctional drugs with high therapeutic efficacy by enhancing the specificity and selectivity for cellular or molecular targets (Becerril *et al*., 2022).

2.3.2.1 Oxygen Carrying Strategies

One of the most common approaches for overcoming tumor hypoxia during photo dynamic therapy is direct oxygen administration into tumor microenvironments. It has been shown that manipulating tumor oxygenation through hyperoxygenation or carbogen, can increase the therapeutic effectiveness of photo dynamic therapy in rodent models and in clinical trials (Larue *et al*., 2019). Many different kinds of oxygen nano-carriers have recently been developed.

2.3.2.1.1 Nanobubbles

Nanobubbles are spherical vesicles consisting of a shell and a gas core (Kheir *et al*.,2012). For safety reasons to prevent hemolysis, free gas should not be administered straight into blood flow. Instead, it has been shown that oxygen can be delivered for tumor oxygenation without adverse effects and to improve tumor treatment, using nano/microbubbles made of a stabilizing monolayered shell made of lipids or polymers and an oxygen-carrying gas center (Iijima *et al*., 2018, Song *et al*., 2018 & Owen *et al*., 2016).

According to their hydrophobic or hydrophilic characteristics, nano/microbubbles can also be drug-loaded by coating the exterior shell or encapsulating the center (Khan *et al*., 2019). The nano/microbubbles can be made to regulate the oxygen release in response to external cues in order

to prevent premature oxygen release and minimize side effects. The stability and storing problems of oxygen nano/microbubbles remain difficult despite major advancements.

2.3.2.1.2 Artificial Red Blood Cells

The natural oxygen carrier in our body is hemoglobin (Hb), which is found inside red blood cells (RBC) and has four heme groups that firmly bond to oxygen. However, due to its poor stability, which would later result in severe renal toxicity, free Hb is not a viable choice for delivering oxygen (Pawlowski *et al*., 2013). As a result, a variety of Hb-based nanomaterials—often referred to as "artificial RBCs"—have been created and it has been demonstrated that they are extremely effective at treating tumor ischemia. Although Hb has excellent biocompatibility, the use of artificial RBCs is restricted due to its low oxygen transport efficacy (each Hb has only four oxygen binding sites) (Shih *et al*., 2021).

2.3.2.1.3 Perfluorocarbons

The organofluorine compound perfluorocarbons (PFCs) has the formula CxFy. Fluorine has a very low polarizability, which makes PFCs very gas soluble. Their oxygen transporting capability is 1.5 times greater than that of Hb. Additionally, the Food and Drug Administration (FDA) of the United States has authorized PFCs for parenteral use as a synthetic blood replacement. PFCs have a high oxygen carrying capability, but their superhydrophobic properties prevent their use in tumor treatment. Fortunately, this issue can be resolved using different nano formulations, such as porous nanoparticles (NPs) (Shih *et al*., 2021).

2.3.2.1.4 Nanoscale metal-organic frameworks

Nanoscale metal-organic frameworks (nMOFs) are a type of porous nanomaterial with consistent pore size and large surface area and they have a significant potential for gas storage, particularly for oxygen (Li *et al*., 2016, DeCoste *et al* 2014 & Zhang *et al*., 2020). Additionally, nMOF's multipurpose qualities based on the adaptable cargo design make it an excellent option of transport for oxygen-enhanced photodynamic therapy, loading photosensitizers with oxygen (Gao *et al*., 2018). The tunable property of nMOFs makes them intelligent carriers that can discharge oxygen cargos selectively. In addition to transporting oxygen directly, nMOFs have the ability to move PFC cargos that distribute oxygen (Wanigarathna *et al*., 2020).

2.4 Nanobubbles

Nanobubbles are microscopic bubbles that develop in liquid solutions and at solid-liquid interfaces when insoluble gasses like oxygen, nitrogen, carbon dioxide, hydrogen, and helium interact with one another. They can move from the vasculature to the extravascular target location, considerably expanding the application range of ultrasonic molecular imaging. Nanobubbles can also be used to load drugs or genes for therapeutic purposes, similar to microbubbles. As a result, they are frequently utilized for medication and gene delivery as well as ultrasonic molecular imaging. Nanobubbles may be utilized as a probe in ultrasound molecular imaging of a variety of disorders, such as tumor allograft rejection, and others when conjugated with certain ligands (Zhang *et al*., 2019).

2.4.1 Shell Types

Depending on the kind of casings and core gas used, the stability and biocompatibility of MNBs and the discharge of core gas will vary (Khan *et al*., 2018). In addition to providing stability and defense against endogenous scavengers, the shell slows the rate of diffusion of the core gas into the surrounding media (Fix *et al*., 2015). The stiffness, elasticity, gas exchange, half-life, resistance to applied ultrasonic pressure and ease of excretion of MNBs from the body are all influenced by the shell composition (Cavalli *et al*., 2013). Soft shells are more likely to shatter than hard ones whereas rigid shells cannot oscillate in ultrasonic environments (Cavalli *et al*., 2013). The composition of the shell is an essential component in the loading of drugs and genes. Therefore, it is important to choose appropriate shell materials for diverse applications of MNBs with various thicknesses, stiffnesses, charges and functional groups (Martin *et al*., 2013). MNBs have a shelf life that varies based on the kind of shell substance used, from a few weeks to several months. Various methods have been used to lengthen the storage life. The *in vivo* half-life of MNBs varies based on the chemical composition of the shell from a few seconds to several hours (Khan *et al*., 2018). Below is an overview of the key characteristics of the different kinds of shells.

2.4.1.1 Lipid Shells

Since they are biocompatible and biodegradable, lipid-based nanoparticles and microparticles are favored for medical uses. These lipid shells exhibit better resonance under acoustic pressures and enable gas to move through the shells. Due to their amphiphilicity and

hydrophilic head and hydrophobic ends, phospholipids are commonly used in lipid-shelled MNBs (Li *et al*., 2015). At the gas-water contact, phospholipids can self-assemble into monolayers and the gas or hydrophobic medicines can be enclosed within these lipid shells (Kheir *et al*., 2012). Lipids have a great degree of cohesion, giving these MNBs solid-like properties. The kind of lipids used affects how stiff the lipid layers are. The stiffness of the shells is increased by longer hydrocarbon chains (Cavalli *et al*., 2013). With the right amount of emulsifiers, lipid-coated MNBs can be functionalized.

2.4.1.2 Protein Shells

Protein-shelled MNBs have advantages over other MNB types in terms of stability, biocompatibility, biodegradability, amphipathic character and extended half-life (Cavalli *et al*., 2013). By emulsifying the protein solution and boiling it to the point of denaturation, protein-shelled MNBs can be produced. Over the ideal gas, the denatured protein creates a narrow monolayer coating (Cavalli *et al*., 2013 & Upadhyay *et al*., 2017). Because the protein casings are rigid, there is little room for dispersion. The disulfide linking that takes place between the cysteine thiol groups may help to explain this stiffness (Fix *et al*., 2015). MNBs with albumin shells have been used as an ultrasonic contrast material.

2.4.1.3 Polymer Shells

Polymer shell bubbles can be up to 200 nm thick. Hence, they are larger than lipid and protein shells and can hold more hydrophobic and hydrophilic medicines than lipid and protein shells can (Khan *et al*., 2018). When ultrasound beams are used, polymeric shell droplets are more impervious to deformation and expansion (Cavalli *et al*., 2013). When greater pressures are applied, they fracture or defect and show low oscillations, which allows the gas or substance to spread out. Researchers have also used biodegradable materials to carry oxygen. The durability, biocompatibility, uniformity, biodegradability and purity of cellulose, chitosan, poly (lactic acid), poly (vinyl alcohol), poly (glycolic acid) and poly (lactic-co-glycolic acid) (PLGA) have led to their use in the creation of polymeric shell MNBs (Cavalli *et al*., 2013).

2.4.2 Characterization Techniques

Various characterization techniques have been applied to characterize MNBs. Micron-sized bubbles can be seen using optical and fluorescence imaging and the size of the nanobubbles can be determined using dynamic light scattering (DLS) and other optical particle counts (Kheir *et al*., 2012, Fix *et al*., 2015 & Legband *et al*., 2015). MNBs have been viewed using transmission electron microscopy (TEM) and scanning electron microscopy (SEM) methods (Kheir *et al*., 2013). Electrochemical sensing, fiber optic-based sensing and fluorescence quenching are techniques for measuring liquid oxygen (Zhao *et al*., 2014). When cells are hypoxic, fluorescence quenching is a live cell imaging method that can be used to assess how well MNBs work to restore hypoxia (Khan *et al*., 2018).

2.4.3 Synthesis of Nanobubbles

MNBs are synthesized by various methods. Some of them include ink jet method, laser ablation, emulsification, agitation, microfluidic method and sonication method (Matsuki *et al*., 2012).

2.4.3.1 Ink Jet Method

Depending on the application, a piezo-driven ink-jet nozzle of a desired size is used to force a polymer solution through. The solution is pulsed by the piezoelectric crystals and the resulting bubbles are expelled from the opening (Lee *et al*., 2015). By using a high-pressure passage through the nozzle, a similar technique has also been used to produce ultrafine oxygen nanobubbles from purified water and an oxygen source (Iijima *et al*., 2018).

2.4.3.2 Laser Ablation Method

Aluminum oxide particles in water can be targeted by an excimer laser of a specific frequency, generating oxidized nanoparticles as a result. At the solid-liquid contact, bubbles will also be created during the procedure. The aluminum oxide nanoclusters stabilize the bubbles/interface (Lee *et al*., 2015).

2.4.3.3 Emulsification Method

In this procedure, an oil and carrier polymer create an emulsion that contains water and this emulsion is then further mixed in a sizable amount of water. To create a solid polymer shell,

the solvent is removed or vaporized. Lyophilized polymer shells are then filled with core gas, like PFCs. A technique of high-shear emulsification has been used to create MNBs with a wider variety of sizes (Matsuki *et al*., 2012). MNBs with a limited size range can be produced by a membrane emulsification technique. For this, a permeable barrier is employed. Along the membrane surface, a constant phase of gas molecules permeates and disperses. To avoid coalescence, emulsifiers are introduced (Khan *et al*., 2018).

2.4.3.4 Agitation Method

MNBs are produced by shaking the watery solution at several thousand vibrations per minute, particularly those with lipid shells. A random height distribution of bubbles will result from this (Cavalli *et al*., 2016). The desired coating material is added to the container in the liquid phase, the desired gas is perfused from the top and then the container is manually stirred to ensure that the desired gas is completely encapsulated by the shell material (Cavalli *et al*., 2016).

2.4.3.5 Microfluidic Method

Gas and shell material in liquid state will be forced to collide with each other at T junction and result in nanobubble formation. The mechanism behind this formation is not fully known. The following are the two primary techniques for creating microfluidic devices: (1) Flow focusing units made using soft lithography methods and (2) manually constructed units made from capillaries assembled in a polymeric block. In both situations, the vapour and liquid move into a T-junction. Depending on the device's opening size and other factors, the MNBs are then produced in the T-junction (Cavalli *et al*., 2016). The size and distribution of the MNBs can be regulated by varying the flow rate, pressure, liquid solution viscosity and device orifice size (Cavalli *et al*., 2016).

2.4.3.6 Sonication Method

For the production of MNBs of various types of outer coverings, including lipids, polymers, proteins and surfactants, sonication is used. High-pressure and low-pressure regions in the fluid result from compressions and rarefactions caused by ultrasonic application. Additionally, if surfactants or coating materials are present in the medium, the ultrasonic pressure may destroy them, leading to their transformation into new forms, stabilizing the gas-liquid contact by the creation of MNBs (Cavalli *et al*., 2016 & Lee *et al*., 2015). It is not completely understood how

cavitation and bubble formation work. However, sonication factors like frequency, pulse duration and strength can be used to regulate the size distribution (Leon *et al*., 2018). The output and production of MNBs are the method's limitations. This is due to the fact that a finite quantity of solution can be sonicated in a finite amount of time.

2.4.4 Application of Nanobubbles

2.4.4.1 Biomedical Imaging

2.4.4.1.1 Ultrasound Contrast Enhancement

Due to the compressibility of the encapsulated gas, gas bubbles within tissues can function as harmonic oscillators, oscillating/resonating in reaction to ultrasound stimulation (Leon *et al*., 2018). When bubbles are present in tissues, the second harmonic causes backscattered ultrasound signals to become more intense than they would be in surrounding tissue (Exner *et al*., 2021, Batchelor *et al*., 2021, Favvas *et al*., 2021 & Cui *et al*., 2013). Microbubbles have been used by scientists and doctors for years to increase the ultrasound strength in blood pool imaging, but nano-scale contrast agents have distinct advantages that micro-scale agents cannot match (Jin *et al*., 2015 & Conversano *et al*., 2012). Because of the enhanced permeability and retention effect, nanoscale drugs are specifically tiny enough to extravasate from the permeable tumor vasculature (Yang *et al*., 2015).

2.4.4.1.2 Photoacoustic Contrast Enhancement

The photoacoustic effect is used in photoacoustic imaging methods to create a picture of the target tissue. Short wave light pulses are used to activate chromophores, optically absorbent molecules in tissue that cause tissue thermoelastic expansion, in order to use this phenomenon therapeutically. An ultrasound transducer senses the resulting pressure pulse and uses that information to determine the location of the chromophores. The distinct physical properties of nanobubbles can be advantageous for photoacoustic imaging as well (Kim *et al*., 2015, Kuriakose *et al*., 2021 & Rodera *et al*., 2018). Chromophores can be enclosed within microbubbles and nanobubbles, extending their half-life in the bloodstream and decreasing the chemical interactions between chromophores and proteins that could result in erratic spectral properties (Xu *et al*., 2011).

2.4.4.1.3 Molecular Imaging

Molecules that have an affinity for indicators on target organs or cells can be used to functionalize nanobubbles. Then, using their contrast-enhancing characteristics, the nanobubbles are tracked spatiotemporally *in vivo* to show the activity of the target tissues or cells using ultrasound or photoacoustic imaging (Zhang *et al*., 2013, Thakor *et al*., 2013 & Liu *et al*., 2018). This method can be used to monitor the molecular alterations that go along with cancer growth and metastasis and to foretell the best treatment plan for various tumor kinds (Yu *et al*., 2020 & Perera *et al*., 2020).

2.4.4.2 Dentistry

Dentistry uses stem cell regeneration to address tooth-related illnesses and conditions. One area of dentistry that could benefit from bulk nanobubbles is the *in vitro* culture of human dental follicular stem cells (DFSCs). Although the cause of this occurrence is still unknown, the air/oxygen nanobubbles may change the cells' development behavior. The presence of air/oxygen nanobubbles in the culture media of DFSCs improves the proliferation of DFCSs (Oishi *et al*., 2018).

The Therapy of periodontal disorders is another use for bulk nanobubbles in dentistry. Arakawa *et al*. (2017) treated patients with peri-implantitis-related bone loss and inflammation using a water and ozone nanobubble solution. Ozone nanobubble irrigation of the impacted region for 12 weeks significantly decreased the amount of bacteria present, eliminating inflammation and restoring the injured bone.

2.4.4.3 Gene Delivery

As a non-viral vector gene delivery system, ultrasound-mediated gene delivery systems with nanobubbles have been developed recently. In this method, the cell membrane is disrupted by using nano- and micro-bubbles that combine with ultrasound to create temporary pores. Because of this, endocytosis is not required for the transmission and transduction of genetic information into the host cell. This technique is beneficial because it uses ultrasound to manipulate and expose specific tissues and organs with therapeutic genes in a non-invasive and tissue-specific manner (Xiong *et al*., 2021).

2.4.4.3.1 Plasmid DNA Delivery

The transfection technique, which involves subjecting cells suspended with microbubbles and plasmid DNA to ultrasonication for up to tens of seconds, has been used in *in vitro* experiments before (Xiong *et al*., 2021). Here, ultrasound exposure parameters like strength, frequency, duration, duty cycle, type and microbubble concentration have an impact on transfection efficacy. However, optimal circumstances for maximizing transfection efficacy are not well known.

2.4.4.3.2 Oligonucleotide Delivery

Short single- or double-stranded nucleic acid molecules known as oligonucleotides have the ability to inhibit the production of a particular gene and could eventually be utilized to create novel therapies for autoimmune, infectious and malignant illnesses (Xiong *et al*., 2021). Common oligonucleotides like antisense, decoy and siRNA must reach the specific cells' cytoplasm in order to achieve efficient gene silencing. It has been discovered that combining ultrasonic and nanobubbles is an efficient way to transport extracellular molecules into the cytoplasm, where oligonucleotides work best (Suzuki *et al*., 2011).

2.4.4.4 Tumor Ablation

High intensity focused ultrasound (HIFU), radiofrequency irradiation, microwave irradiation, laser irradiation, cryoablation and permanent electroporation are examples of techniques used in thermal ablation to temporarily raise the temperature of target tissues and cause coagulative necrosis (Knavel *et al*., 2013). These methods are frequently used to handle incurable malignancies of the liver, pancreas, bone, kidney and lung non-invasively (Knavel *et al*., 2013, Lee *et al*., 2013 & Zhang *et al*., 2015). Multiple studies have demonstrated that bulk nanobubbles can enhance the efficacy of HIFU by increasing the acoustic energy deposition in target tissues as a result of shear stress, cavitation and streaming caused by nanobubble oscillation and collapse, as well as by the controlled release of thermal sensitizers and anti-cancer drugs to the tumor (Perera *et al*., 2013, Suzuki *et al*., 2016 & Zhang *et al*., 2014).

2.4.4.5 Oxygen Delivery

Oxygen nanobubbles (ONBs) are newly invented nanomaterials that can provide oxygen to developing tissues and cells. It is possible to produce supersaturated fluids for the delivery of

oxygen using nanobubbles (Khan *et al*., 2019). In wastewater treatment, oxygen nanobubbles have also been used to degrade organic pollutants and detoxify water (Wang *et al*., 2009). Most of the research surrounding nanobubbles, aims to deliver oxygen and drugs within tumor cells to aid chemotherapy.

2.4.4.5.1 Wound Healing

Oxygen is vital for healing wounds. It is intricately involved in numerous biological processes including cell proliferation, angiogenesis and protein synthesis which are required for restoration of tissue function and integrity. The main causes of low oxygen levels that frequently result in cellular toxicity are hypoxia and ischemia-reperfusion. A substitute for the conventional treatments is utilizing oxygen nanobubbles, as their stability in solution helps increase the oxygen level in a wound over an extended time. Another advantage is their ability to trap a volume of oxygen, which can provide sufficient oxygen for the treatment by injecting them into the damaged tissue. In addition to the oxygen delivery benefits, the negative surface charge of oxygen nanobubbles attracts debris and enhances the cleaning of the wound (Sayadi *et al*., 2018).

2.4.4.5.2 Tumor Hypoxia Treatment

Tumor hypoxia can cause cancer cell survival in hypoxic regions (Bao *et al*., 2021). In addition, hypoxia worsen the efficacy of standard cancer treatments such as radiation and photodynamic therapy. One possible way to oxygenate tumor cells is the use of lipid coated oxygen nanobubbles. Lipids in the nanobubble shell increase stability and prevent the release of oxygen before it reaches the tumor while using it. Nanobubble release of oxygen cargo is controllable and can be performed by ultrasonic stimulation (Cao *et al*., 2018).

This study was taken up to synthesize oxygen nanobubbles by sonication and characterize them to determine their morphology, size, surface charge, surface area, dissolved oxygen content and elemental composition. These nanobubbles were then assessed for their ability to reverse acute hypoxia in rats.

3.0 EXPERIMENTAL PROCEDURE

The Experimental Procedure pertaining to the study entitled **"Coagulation Proteins in Rats during Hypoxia Reversal by Oxygen Nanobubbles"** is discussed under the following headings:

3.1 Synthesis of Sodium Carboxy Methyl Cellulose Oxygen Nanobubbles (SCMC-ONB)

Several processes are used to prepare nanobubbles. Common techniques include laser ablation, microfluidic devices, agitation and sonication. Sonication is one of the quickest methods for producing nanobubbles. This method can be utilized to create NBs from various materials such as lipids, polymers, proteins and surfactants (Cavalli *et al*., 2016).

Sonication produces nanobubbles of varying sizes, since it is a stochastic process. However, the sonication parameters, such as frequency, pulse duration and strength, can be used

to regulate the size distribution (Stride *et al*., 2008). In the present study, oxygen nanobubbles were produced by the sonication of sodium carboxymethyl cellulose (SCMC) using a probe sonicator and bathtub sonicator. Different trials were carried out with varying concentrations of SCMC. Different aqueous solutions were also used to prepare nanobubbles. Table 1 contains the combinations used to prepare nanobubbles. The detailed procedure is described in Appendix I.

Table 1

Combinations for Nanobubble Preparation

Sonicator	Duration of Sonication (minutes)	Conc. of SCMC (%)	Aqueous solution used	Conc. of Aqueous Solution
Bathtub	10, 20 & 30	0.25	Sodium Chloride	0.5%
Probe Tip	10, 20 & 30	0.25	Sodium Chloride	0.5%
Probe Tip	5, 10 & 15	0.25	Sodium Chloride	0.9%
Probe Tip	10	0.25	Phosphate Buffered Saline	0.1 M
Probe Tip	10	0.5	Phosphate Buffered Saline	0.1 M
Probe Tip	10	0.75	Phosphate Buffered Saline	0.1 M

3.2 Characterization of Oxygen Nanobubbles

Particle size analyzer and Zeta Potential, Scanning Electron Microscopy (SEM), Energy Dispersive X-ray (EDX) analysis, Three-Dimensional optical profiler, Fourier Transform Infrared (FTIR), Dissolved Oxygen (DO) meter, Transmission electron microscopy (TEM) and absorption spectroscopy were used to characterize the produced oxygen nanobubbles.

3.2.1 Particle Size Analysis

Size of the synthesized nanobubbles is determined by Particle Size Analyzer which works on Dynamic Light Scattering (DLS) principle. The DLS technique is based on the scattering of light by diffusing particles. At any instant, particles suspended in solution will have a particular set of positions and will scatter light accordingly. DLS is an established technique that has the

advantage of being fast and non-invasive, but it does require low particle concentrations (Ashizawa, 2019).

DLS is an essential technique for nanoparticle size analysis and has been employed extensively for decades. In recent years, for instance, more than 50% of drug products containing nanomaterials submitted to the Center for Drug Evaluation and Research within the US Food and Drug Administration relied on DLS for size characterization (Farkas *et al*., 2021). The detailed procedure for DLS is described in Appendix II.

3.2.2 Zeta Potential

Any particle in suspension, macromolecule or material surface exhibits the physical characteristic known as zeta potential which depicts the charge on the surface. The surface zeta potential of nanobubbles was measured using a zeta potential analyzer to characterize the surface charge of nanobubbles in solution under different conditions. Applying an electric field across the dispersion allows one to measure the zeta potential of the dispersion. The colloidal system's potential stability is indicated by the zeta potential's magnitude (Calgaroto *et al*., 2014).

The different values of zeta-potential may indicate different stability of the nano-bubbles according to the type of gas, as well as different structures at the gas-liquid interface. Many reports in the literature discuss the difficulty of measuring the zeta-potential in a dispersion of bubbles because of the interference of the gravitational field and of the lack of stability of the bubbles during the measurements. In the case of nanobubbles, the long residence time in the liquid due to the low rising velocity of the bubble is an advantage in the zeta-potential measurement (Ushikubo *et al.*, 2010). The detailed procedure for Zeta potential measurement is described in Appendix III.

3.2.3 Dissolved oxygen content

An important sign of an ONB's capacity to release oxygen is the amount of dissolved oxygen. They also aid in assessing sample quality (Wei *et al*., 2019). Measurements of the amount of gaseous oxygen dissolved in samples are made using dissolved oxygen meters. After injecting oxygen containing nanobubbles into a deoxygenated fluid, electrochemical sensing has also been used to determine the amount of dissolved oxygen in the liquid (Wei *et al*., 2019). The detailed procedure is described in Appendix IV.

3.2.4 Field Emission Scanning Electron Microscopy - Energy Dispersive X-Ray

Field Emission Scanning Electron Microscopy is also known as a field emitter (FESEM), which produces better images, when a cathode releases electrons while being subjected to a very strong electric field (Owen *et al.,* 2016). With nearly infinite depth of field and magnifications ranging from 10X to 300,000X, FESEM offers topographical and elemental data. With a spatial resolution as well of 1 1/2 nanometers, FESEM creates images that are clearer and less electrostatically distorted (Mayeen *et al*., 2018).

An X-ray technique called Energy Dispersive X-Ray Analysis (EDX), often known as EDS or EDAX is used to determine the chemical make-up of substances. Both qualitative and quantitative analysis can be done with it. The distribution of the atoms in our samples can also be mapped, in addition to measuring the relative amounts of each atom (Scimeca *et al.*, 2018). In the present study, Field Emission Scanning Electron Microscopy - Energy Dispersive X-Ray (FESEM-EDX) study using a QUANTAX EDS SOP BRUKER was used to look at the surface morphology and to determine the elemental composition of the SCMC-ONB. The detailed procedure is described in Appendix V.

3.2.5 Fourier Transform Infrared Spectroscopy (FTIR)

Infrared spectroscopy is most commonly performed using the Fourier transform. It is a general analytical instrument to determine functional groups of a variety of materials, particularly for identifying unidentified compounds. When proper standards are used, FTIR analysis can be used to analyze materials quantitatively as well as qualitatively. A wide range of materials, including bulk or thin films, liquids, solids, pastes, powders, fibers and other substances, can be analyzed using FTIR (Othman, 2022). Hence, FTIR was used to characterize oxygen nanobubbles and their peak values were utilized to identify functional groups. In this study, the presence of functional groups in SCMC-ONB was determined using a Nicolet 6700 FT-IR Spectrometer. The detailed procedure is described in Appendix VI.

3.2.6 Three-Dimensional Optical Profiler

A technique for obtaining topographical data from a surface is 3D profilometry. Surface morphology, step height and surface roughness are all assessed by this technique. Clear information on the precise topographical data is provided by 3D optical profiling. This particular

type of microscope uses light that enters the material directly to determine the degree of surface roughness. It is possible to use a single point, a line scan, or even a complete three-dimensional scan (Kaplonek *et al*., 2020). In the present study, analysis was performed utilizing a Contour X - 100 to look into the surface area and roughness of SCMC-ONB. The detailed procedure is described in Appendix VII.

3.2.7 Transmission electron microscopy (TEM)

Numerous studies have already been carried out with the main goal of characterizing nanobubbles by transmission electron microscopy (TEM). A "Philips CM10" Transmitting electron microscopy was used to analyze the three-dimensional structure of nanobubbles. Formulations for nanobubbles were dropped onto a Formvar-copper grid coated with for TEM investigation, then allowed to air dry before being seen. Additionally, measurements of average diameters and shell thickness were made using TEM images (Argenziano *et al.,* 2022). The detailed procedure is described in Appendix VIII.

3.2.8 Absorption spectrum

UV-Visible absorption spectroscopy is a method for measuring the amount of light that is absorbed and dispersed by a substance. Absorption spectroscopy determines how much light a sample absorbs over a range of wavelengths defined by electromagnetic spectra. The wavelength at which a chemical component absorbs light depends on the sort of ion or molecule being measured. The Beer Lambert rule states that the amount of light absorbed is proportional to the pathlength and concentration of the substance. Light and chemical interactions can occur in many different kinds of ways, with each kind frequently happening within a particular wavelength range. In its most basic configuration, a sample is positioned between a light source and a photodetector and the intensity of a light beam is assessed both before and after it passes through the sample. To determine the sample's wavelength dependent extinction spectrum, these measurements are contrasted at each wavelength. Usually, the data is presented as an extinction function of wavelength.

Size, shape, concentration, aggregation state and refractive indices close to the nanoparticle surface all affect the optical properties of nanoparticles. As a result, UV-Visible spectroscopy is a useful tool for identifying, describing and researching these materials (Mochalov *et al*., 2019).

3.3 Animal Study

This study was designed to assess the ability of the oxygen nanobubbles to reverse hypoxia in the animal model rats. The aim of this study is to utilize nanobubbles to treat hypoxic conditions in humans. Albino rats serve as the best model organism for humans as they have both genetic and physiological similarities to human beings.

3.3.1 Ethical approval

This animal study was approved by the Institutional Animal ethics committee (IAEC) of the Avinashilingam Institute (AIW:IAEC.2023:12). Each of the experiments were carried out adhering to the appropriate rules and regulations prescribed by the IAEC.

3.3.2 Induction and treatment of hypoxia in Rats

15 male albino rats which were 12 – 15 weeks old were weighed and chosen for the experiment. The animals were housed in the Animal House of Avinashilingam Institute for Home Science and Higher Education for Women, Coimbatore. They were fed with *ad libitium* food and water. The animals were divided into 5 different groups shown in Table 2.

Table 2

Experimental Groups

Groups	Treatment Given	No. of Animals in Each Group
Group 1	Hypoxia control	3
Group 2	Hypoxia + 100µl of SCMC-ONB	3
Group 3	Hypoxia + 200µl of SCMC-ONB	3
Group 4	Hypoxia + 500µl of SCMC-ONB	3

The Group 1 rats were considered as hypoxia control. Hypoxic condition in rats was induced by administering 1 ml of ketamine/animal. The oxygen saturation and pulse rate were

monitored for about one hour after ketamine administration. Blood was drawn from each rat through heart puncture and collected in EDTA tubes/trisodium citrate tubes/clot activator tubes to perform enzyme assays/blood count/estimate coagulation factors. Serum was separated from the blood using the clot activator tubes. Plasma was collected by centrifuging the blood collected in the trisodium citrate tubes. The complete blood count test was performed using the blood from EDTA tubes.

After induction of hypoxia, in groups 2, 3 and 4 rats were administered with 100µl, 200µl and 500µl of SCMC - ONB, respectively. Ketamine was administered to induce hypoxia in rats. After 10 minutes of ketamine administration, the respective amount of oxygen nanobubbles were administered through the tail vein. After one hour of monitoring oxygen saturation and pulse rate, blood was drawn from each rat through heart puncture and collected in EDTA tubes/trisodium citrate tubes/clot activator tubes to perform enzyme assays/blood count/estimate coagulation factors. Serum was separated from animal blood using the clot activator tubes by centrifugation. Plasma was collected by centrifuging the blood collected in the trisodium citrate tubes. The complete blood count test was performed using the blood from EDTA tubes.

3.3.3 C Reactive Protein Assay

C Reactive Protein (CRP) is an acute phase protein synthesized in the liver. Its rate of synthesis increases within hours of acute injury or the onset of inflammation and may reach as high as 20 times the normal levels. A rapid fall of CRP indicates recovery. The degree of elevation of CRP level directly reflects the mass or activity of inflamed tissue. The degree of inflammation caused by hypoxia is assessed using the procedure outlined by Thomas *et al*. (1998), and is detailed in Appendix IX.

3.3.4 Fibrinogen Assay

Fibrinogen (Factor I) is a high molecular weight glycoprotein synthesized in the liver, which plays an important role in hemostasis. For normal hemostasis to occur in response to injury or tissue damage, a sufficient concentration of fibrinogen must be present in plasma. The fibrinogen levels increase due to tissue damage or injury (Bekos *et al*., 2017). The amount of fibrinogen in the blood serum corresponds to the level of turbidness that can be measured at

wavelength 340 nm. The level of Fibrinogen in rats was measured using the protocol elaborated by Thomas *et al*. (1998) and is given in the Appendix X.

3.3.9 D-Dimer Assay

During coagulation, a sequence of reactions occurs in the body in response to a variety of external and internal stimuli. The enzymatic cascade reaction terminates in the conversion of fibrinogen to fibrin, by the enzyme thrombin. The fibrin gel is then converted to a stable fibrin clot by thrombin activated factor XIII. The fibrin network is dissolved by the enzyme plasmin to generate cross-linked degradation products. D-Dimer, consisting of two fragments crossing together, is the smallest plasmin resistant molecular unit present within the cross-linked products. D-dimer assay is carried out to assess the fibrin formation which results in blood coagulation. The estimation is done as an immunoturbidimetric assay in human plasma by following the protocol of Hirsh *et al*. (1994), as shown in Appendix XI.

3.4 Statistical Analysis

Means and standard deviation were calculated from the data and analyzed using one-way analysis of variance (ANOVA), for comparisons between multiple groups, significance is reported at $p < 0.5$. Tukey HSD (honestly significance difference) test was used to identify which groups were significantly different from each other. Unpaired Student's T test was carried out to analyze the assay results and significance is reported at $p < 0.5$.

4.0 RESULTS AND DISCUSSION

The Results and Discussion pertaining to the study entitled "**Coagulation Proteins in Rats during Hypoxia Reversal by Oxygen Nanobubbles**" is discussed under the following headings:

4.1 Synthesis of oxygen nanobubbles

4.2 Characterisation of Oxygen Nanobubbles

- **4.2.1 Particle Size & Zeta Potential**
  - **4.2.1.1 Trial 1**
  - **4.2.1.2 Trial 2**
  - **4.2.1.3 Trial 3**
- **4.2.3 Dissolved Oxygen Content**
- **4.2.3 Scanning electron Microscopy**
- **4.2.4 Energy Dispersive X-Ray Spectroscopy**
- **4.2.5 Fourier Transform Infrared Spectroscopy**
- **4.2.6 Three-Dimensional Optical Profiler**
- **4.2.7 Transmission Electron Microscopy**
- **4.2.8 Absorption Spectrum**

4.3 Animal Studies

- **4.3.1 Oxygen Saturation**
- **4.3.2 Biochemical Studies**
  - **4.3.2.1 Acute Phase Protein**
    - **4.3.2.1.1 C – Reactive Protein Levels**
  - **4.3.2.2 Blood coagulation proteins**
    - **4.3.2.2.1 Fibrinogen Levels**
    - **4.3.2.2.2 D-Dimer Levels**

4.1 Synthesis of oxygen nanobubbles

In the present study, synthesis of oxygen nanobubbles was carried out by using sodium carboxymethyl cellulose-a polymeric shell, by sonication method, as shown in Figure 1. The synthesis was carried out with different concentrations and with different aqueous solutions

as depicted in Tables 3, 4 and 5. During sonication, the solution turned milky in colour and after the process the liquid obtained was a clear colourless solution. The colour change is depicted in Figure 1. The colour change may be due sonication and formation of nanobubbles.

Figure 1

SCMC oxygen nanobubble prepared using sonication method

Before **After**

MNBs have been produced by researchers using pulsed sonication at 100 to 200 W for 1 to 5 minutes (McEwan *et al*., 2015). The sonication method is suitable for the laboratory scale of nanobubble production; large volumes of samples cannot be prepared using this method. Researches are made to innovate new methods that can yield nanobubbles on a large scale.

4.2 Characterisation of Oxygen Nanobubbles

Oxygen nanobubbles prepared are standardised by characterising their features for size, oxygen release, surface morphology and elemental composition by various methods. The results obtained for the characterisation are discussed here.

4.2.1 Particle Size Analysis & Zeta Potential

4.2.1.1 Trial 1

The oxygen nanobubbles were analysed using the particle size analyser to assess the size of the nanobubbles and also the size dispersion of the nanobubbles in the solution. Sonication process can be done using a probe tip sonicator or bath tub sonicator. Table 3 contains the nanobubble characteristics prepared using a bathtub sonicator and probe tip sonicator. 0.25 % SCMC and 0.5 % NaCl were used for nanobubble preparation. Polydispersity index (PDI) is a measure of heterogeneity of a sample based on size. Nanobubble sizes, PDI values and zeta potential obtained from prepared nanobubbles for the first trial, shown in the Table 3.

Table 3

SCMC Nanobubbles using Probe Tip and Bathtub Sonicator

Type of Sonicator	Duration of Sonication (min)	Diameter (nm)	PDI	Zeta Potential (mV)
Probe tip	10	97	4.64	-20.5
Bathtub		431	1.80	- 6.5
Probe tip	20	270	2.07	-14.3
Bathtub		288	1.73	- 6.5
Probe tip	30	319	1.48	-22.6
Bathtub		156	2.62	-14.6

Nanobubbles were prepared using both probe tip and bathtub sonicator for different time periods: 10, 20 and 30 minutes. The nanobubbles prepared using the bathtub sonicator have a

diameter ranging from 150 - 450 nm, whereas the nanobubbles prepared using probe tip sonicator have a diameter ranging from 90 - 320 nm. According to Banche *et al*. (2022), light scattering measurements showed that oxygen-loaded nanobubbles (OLNBs) and oxygen fluorescent nanobubbles (OFNBs) had typical dimensions of 700 nm and 300 nm, respectively, in the nanometer range. The size of the nanobubbles prepared are sufficient and might be beneficial for the present application, i.e., oxygen delivery.

On increasing the duration of sonication in probe tip sonicator, the nanobubble size is increases whereas the nanobubble size decreases in bathtub sonicator. The polydispersity index (PDI) decreases on increasing the duration of sonication process in probe tip but it is vice versa in case of bathtub sonicator. Nanobubbles prepared using both the sonicators are polydisperse in nature. A monodisperse sample will contain PDI value less than 0.5. The zeta potential is nearer to -20 mV for nanobubbles prepared using probe tip sonicator and for nanobubbles prepared using bathtub sonicator it is around -15 to -6 mV. The nanobubbles are more stable when prepared using probe tip sonicator than bathtub sonicator. The type of sonicator and duration of sonication affects the size and the dispersion of the oxygen nanobubbles. Considering the results obtained from Trial 1, probe tip sonicator has been chosen for nanobubble preparation in further trials. Figure 2 is an example of a nanobubble size distribution graph.

Figure 2

Nanobubble Size Distribution of 0.25% SCMC ONB

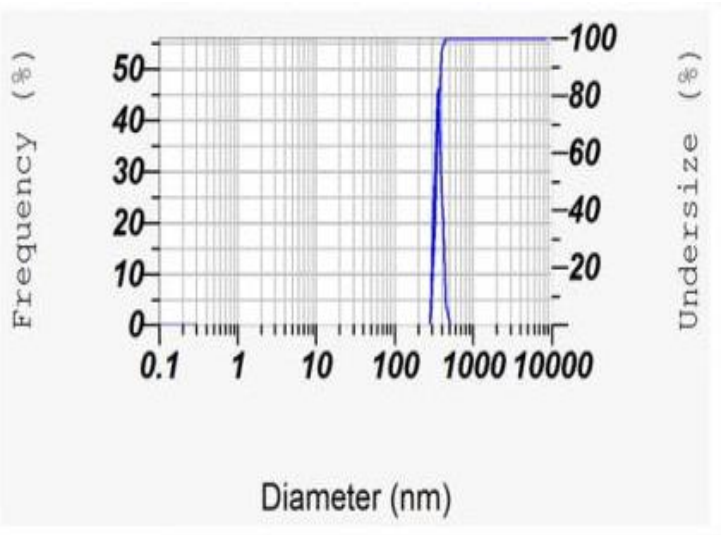

Zeta Potential is to determine the surface charge of the nanobubbles. Nanobubbles are said to be stable only if the surface charge is below -30 mV or above +30 mV. The zeta potential of the prepared nanobubbles is given in Table 3. Figure 3 depicts the graph of zeta potential of 0.25% SCMC ONB.

Xiong *et al*. (2021) synthesised NBs covered with a shell made of poly (lactic-co-glycolic acid) PLGA and oleyl amine. The zeta potential of NBs varied from 11.6 mV (pH 7.4) to 6.2 mV (pH 6.4) and 13.7 mV (pH 5.0) when the pH of the surroundings decreased from 7.4 to 5.0. These findings suggested that the NBs in use had charge-switchable activity that was pH dependent. In order to prevent nanobubble aggregation and ensure that the produced nanobubbles are stable, Zhang *et al*. (2019) proposed nanobubbles that accurately replicated the surface with a negative surface charge that is high. In the present study, the nanobubbles prepared have an unstable nature. However, the zeta potential of nanobubbles produced by probe tip sonicator were less than -14 mV. Since these are much stabler than those produced by bathtub sonicator, further trials were conducted only with probe tip sonicator.

Figure 3

Zeta Potential of 0.25% SCMC ONB

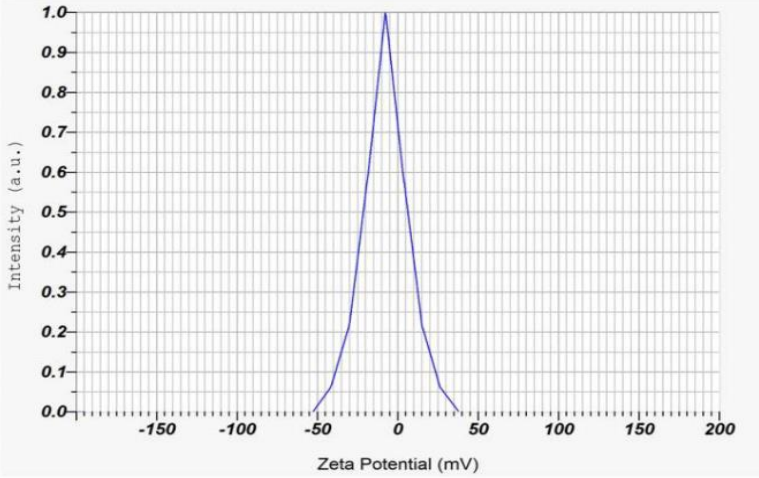

Bhandari *et al*. (2017) discussed about oxygen nanobubbles prepared using carboxymethyl cellulose shell. They anticipated that the non-uniformity of the refractive index caused by the core-shell structure of the nanobubble will cause light to deviate from its linear path and produce light scattering. Localized non-uniformities and the intensity and angular distribution of light scattering are closely related. In order to generate a strong scattering signal from the probes and a high signal to noise ratio, it has gas in an ONB has a refractive index of 1, whereas sodium carboxymethylcellulose shells have a refractive value of 1.515 and phosphate buffered saline background medium has a refractive index of 1.3345. In order to achieve quantitative detection and tracking with single particle resolution, ONB with a significant variation in refractive indices between the shell and the core was produced for this study. The nanobubbles prepared were in the size of 400 nm and 800 nm with 0.37 and 0.63 as their polydispersity index respectively. The PDI seen in Trial 1 were much higher than that observed by Bhandari *et al*., (2017).

4.2.1.2 Trial 2

pH of the aqueous solution used in the production of nanobubbles was assessed. The sample solution containing 0.5% NaCl solution had a pH of 6.6. Since these nanobubbles were prepared to treat hypoxia, they should be isotonic to blood. It is essential for any solution to be administered intravenously to be at pH 7.4.

In the present study, pH 6.6 the nanobubbles prepared had a zeta potential of around –10 to – 20 mV but the results differ from Xiong *et al*. (2021) (6.2 mV). The zeta potential variation is due to change in shell material. The surface charge of the prepared nanobubbles might not be stable but they may be suitable for oxygen delivery to tissues, immediately on administration.

Saline solution (0.9% NaCl) was used as an aqueous solution for nanobubbles preparation in Trial 2. The solution prepared using 0.25% SCMC and 0.9% NaCl was sonicated for various time period (5, 10 and 15 minutes) to produce nanobubbles and they were characterized for their size and surface charge. The results are summarized in Table 4.

Table 4

SCMC Nanobubbles using Saline as Aqueous Solution

Duration of Sonication (min)	Diameter (nm)	PDI	Zeta Potential (mV)
5	295	1.66	-0.3
10	432	0.81	-0.3
15	423	1.19	0.8

Meegoda *et al*., (2018) reported that, the size of nanobubbles increases with increase in salt concentration. After comparing Trial 1 and Trial 2 results, the hypothesis reported by Meegoda *et al*., (2018) is accepted. The nanobubbles are said to be monodisperse when the polydispersity index is less than 1.0 and it is obtained only in nanobubbles sonicated for 10 minutes. So, for further nanobubble preparations 10 minutes of sonication was used. SCMC solution prepared using saline solution had pH 7.0. So, instead of saline, isotonic phosphate buffered saline (PBS) of pH 7.4 was used in next trial. The nanobubble size and surface charge prepared using 0.1M PBS and varying concentrations of SCMC solution sonicated for 10 minutes using probe tip sonicator has been shown in Table 5.

4.2.1.3 Trials 3 & 4

Table 5

Nanobubble Size with PBS as Aqueous Solution

Conc. of SCMC (%) sample	Trial No.	Diameter (nm)	PDI	Zeta Potential (mV)

0.25	Trial 3	325	1.03	- 2.8
	Trial 4	231	1.75	- 0.3
0.5	Trial 3	130	2.65	- 0.4
	Trial 4	122	1.34	- 1.4
0.75	Trial 3	902	0.61	- 1.1

The nanobubble size range obtained in 0.25%, 0.5% and 0.75% are 230 – 330 nm, 120-130 nm and 900 – 910 nm, respectively. The polydispersity index is almost above 1.0, that all the nanobubble preparations are highly heterogenous. The surface charge of nanobubbles from all combinations were in the range of 0 to -3, which depicts the unstable nature of nanobubbles. So, further analysis was carried out to identify the amount of oxygen release by the prepared nanobubbles.

Particle size analysis was also used to determine the size stability of the oxygen nanobubble at different time points such as 0th day, 10th day, 20th day and 28th day after preparation. SCMC ONBs were prepared using 0.5% SCMC and 0.1 M PBS solution and sonicated for 10 minutes and stored at 4°C. On the specified days, nanobubbles were analysed for their size and surface charge. The results are tabulated in Table 6.

Table 6

Nanobubble Stability

Day After Preparation	Diameter (nm)	PDI	Zeta Potential (mV)
0	228	2.05	0.1
10	91	1.60	-0.2

20	60	5.31	-0.3
28	69	8.80	-0.7

Shelf-life study was carried out for a period of 28 days. The size of nanobubbles and surface charge reduces gradually, whereas the polydispersity index increases over the period of time. But the size variations in nanobubbles prepared were much lesser from the size range produced. Bubble size decrease over time due to diffusion of gases out of the bubbles.

Zhang *et al*. (2020) produced nanobubbles and discovered that they are stable in both plasma and saline at 25°C and 37°C for 24 hours, which was supported by photo correlation spectroscopy investigations. After being incubated in plasma, the mean diameter of the nanobubble did not change at a temperature of 25°C. While the stability of nanobubbles at 37°C increased over time, as evidenced by a rise in their diameter.

A dextran shell of around 30 nm was seen in the photomicrographs produced by Khan *et al*. (2019). After being incubated at 25°C and 37°C and diluted in both saline solution and plasma, the oxygen-filled nanobubbles proved to be stable, as shown by TEM and photo correlation spectroscopy investigations. The average sizes of the nanobubbles did not change after being diluted in plasma at 25°C, and both formulations had comparable long-term stability. The analyses showed that the spherical shape and sizes of the nanobubble formulations did not change 24 h after their preparation.

The prepared nanobubbles were unstable for 28 days. But from the above studies it is clear that the nanobubbles are stable up to 24 hours from the time of preparation. The unstable nature may be due to reduced surface charge.

According to Khan *et al*. (2019), for the three composition ratios DSPC, PEG and biotin of 90:5:5, 80:20:0, and 50:50:0, the nanobubble shell composition ratio affects the size, zeta potential, and size distribution. The PEG ratio has increased, which has caused an increase in the zeta potential. The larger positive charge in the situations of 80:20:0 and 50:50:0 might be attributed to the amine derivative present in the PEG surfactant. The 90:5:5 component ratio size distribution range shows two peaks: One is around 50 nm in diameter, while the other has a wide

distribution with a peak at about 10% of the particles between 150 and 750 nm. It is evident that a greater PEG content results in a smaller average size and a narrower size distribution.

Cavalli *et al*. (2009) reported that the diameters of the dextran nanobubble formulations were all less than 1 µm, with a rather homogeneous size range. In order to maintain the surface of the nanobubble, polyvinylpyrrolidone (PVP) forms a hydrophilic coating that may have "stealth-like" qualities when administered *in vivo*. The nanobubbles' surfaces had a negative charge that was strong enough to preclude aggregate formation. The presence of PVP on the nanobubble surface was established since the addition of PVP to the formulation for nanobubbles reduced the zeta potential. From the studies carried out, it is inferred that addition of surfactants like polyethylene glycol, polyvinylpyrrolidone aids in stabilising the prepared nanobubbles. However, in the present study, use of such surfactants may be counterproductive, because of the intended application.

Nanobubbles prepared using probe tip sonicator were more suitable than those prepared using bathtub sonicator, as the nanobubbles prepared using probe tip sonicator were more stable. pH of nanobubbles is important due to their intravenous administration, so isotonic 0.1 M PBS was used as aqueous solution for nanobubble preparation. The nanobubbles of 0.25% and 0.5% SCMC solution were found to be in the size range of 100 - 300 nm but the sizes were not homogenous in nature. With respect to the time period, the nanobubble size decreases and the polydispersity index increases. So, the desired nanobubble characteristics were obtained from combinations of 0.25% and 0.5% SCMC with aqueous solution 0.1 M PBS sonicating them for 10 minutes using probe tip sonicator.

4.2.2 Dissolved Oxygen Content

Dissolved oxygen meter was used to measure the oxygen content in the SCMC ONBs. 1 ml and 10 ml of 0.25% and 0.5% SCMC nanobubbles were introduced to the degassed solution and the oxygen levels were plotted on a graph for 30 minutes and are shown in Figures 4a and 4b.

Figure 4

Dissolved Oxygen Content of Nanobubbles

a) 0.25% SCMC ONB **b) 0.5% SCMC ONB**

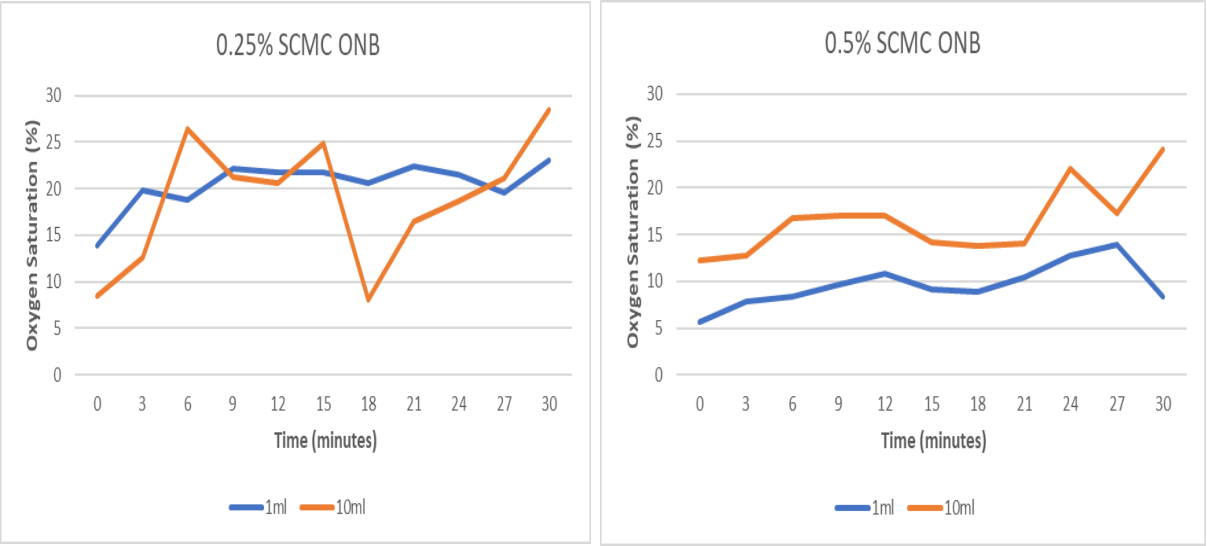

One ml of 0.25% SCMC nanobubbles have high oxygen release in the range of 20 – 25% than 1 ml of 0.5% SCMC nanobubbles in the range of 10 – 15%. When 10 ml of SCMC ONB was used oxygen release in 0.25% SCMC nanobubbles was higher in the range of 25 – 30 % than 0.5% SCMC nanobubbles with 20 – 25% of oxygen release.

Nanobubbles of 0.25% and 0.5% SCMC were analysed for shelf-life study for 5 days from the day of preparation. The readings for the dissolved oxygen content for 0.25% and 0.5% SCMC ONB are listed in Table 7 and shown in Figure 5. The dissolved oxygen content was assessed on each day for to compare the oxygen release characteristics.

Table 7

Dissolved Oxygen Content of 0.25% SCMC ONB

SCMC ONB (%)	Time (minutes)	Day 1	Day 2	Day3	Day 4	Day 5
0.25	0	13.9	18.3	3.30		3.20
0.50		5.6	0.90	2.50	3.10	1.10
0.25	3	19.9	16.0	12.2		5.70
0.50		7.8	15.3	8.55	8.80	2.75
0.25	6	18.8	13.2	9.40		7.75
0.50		8.4	20.90	4.80	10.9	8.30
0.25	9	22.2	13.3	11.5		7.75
0.50		9.7	15.6	5.65	10.8	11.9
0.25	12	21.8	13.8	11.4		10.9
0.50		10.8	21.6	4.5	12.3	10.0
0.25	15	21.8	12.6	13.2		5.55
0.50		9.2	18.0	9.40	10.0	4.70
0.25	18	20.7	12.1	13.4		9.25
0.50		8.9	28.1	10.5	11.6	9.75
0.25	21	22.5	11.7	12.4		7.35

0.50		10.5	27.7	9.00	14.5	1.50
0.25	24	21.5	14.5	12.1		8.80
0.50		12.7	33.4	9.10	8.60	19.3
0.25	27	19.6	11.9	11.8		8.0
0.50		13.9	26.3	5.85	8.70	20.7
0.25	30	23.1	11.7	15.5		8.70
0.50		8.35	18.85	5.5	10.15	20.35

Figure 5

Dissolved Oxygen Content of Stored SCMC-ONBs

a) 1 ml of 0.25% SCMC ONB **b) 1 ml of 0.5% SCMC ONB**

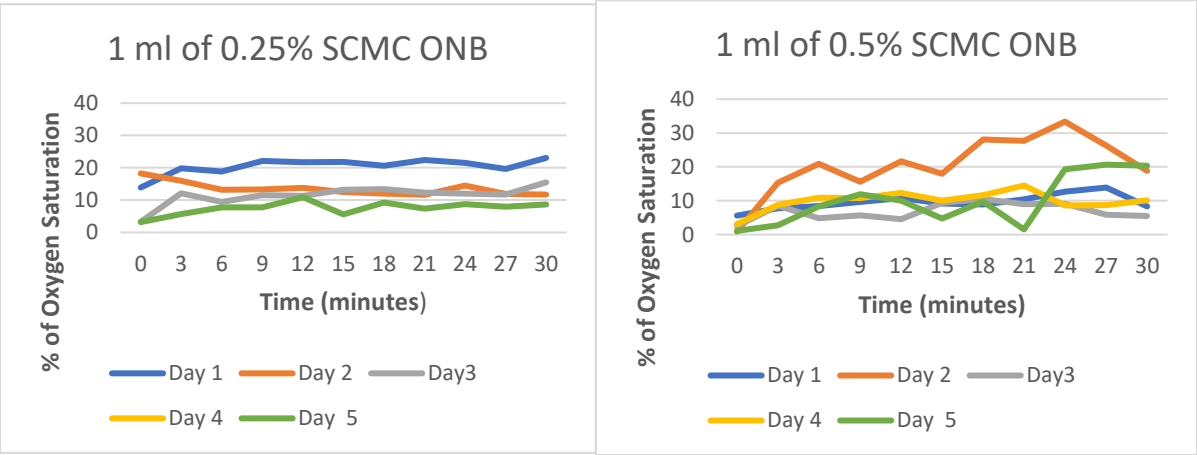

The dissolved oxygen content of each sample varied at different durations. In 0.25% SCMC ONB the dissolved oxygen content was highest on the 1st day and progressively declined till day 5. The highest oxygen release attained was around 30 - 40 %. But in 0.5% SCMC, the dissolved

oxygen content was found to be low on day 1, highest on the 2nd day and then it progressively declined.

Cavalli *et al*. (2009) investigated the effect of ultrasound on oxygen release from nanobubbles. When oxygen concentration in moderate (4 mg/l) and severe (0.4 mg/l) hypoxic conditions were measured 5 minutes after injection of nanobubble formulation, greater amount of oxygen was released in severe hypoxic conditions (0.4 mg/l) than in moderate hypoxic conditions; producing an increase in the oxygen concentration of about 8-fold after 10 min. The oxygen release profiles remained constant for 3 hours following preparation, demonstrating the compositions' durability. The slower oxygen release kinetics, starting from severe hypoxic conditions, are likely caused by the thicker shell.

0.5% SCMC ONB was found to have higher dissolved oxygen when compared to 0.25% SCMC ONB. The highest release of oxygen is seen within 3 – 24 hours of preparation. It might be due to unstable poor layering of shell material, which on rupturing released the oxygen gas.

4.2.3 Scanning electron Micrographs

The SEM analysis provide the details of surface morphology of the nanobubbles. Figure 6 a) and 6 b) shows the surface morphology of 0.25% and 0.5% SCMC ONBs respectively. The images depict that the prepared oxygen nanobubbles are spherical in shape. The FESEM analysis of 0.25% SCMC ONB revealed the diameters of the nanobubbles were found to be in the range of 35 - 66 nm. The diameter of the nanobubbles in the 0.5% SCMC was found to be in a wide range of 31 - 87 nm.

Figure 6

Scanning Electron Micrographs

a) Scanning Electron Micrograph of 0.25% SCMC-ONB

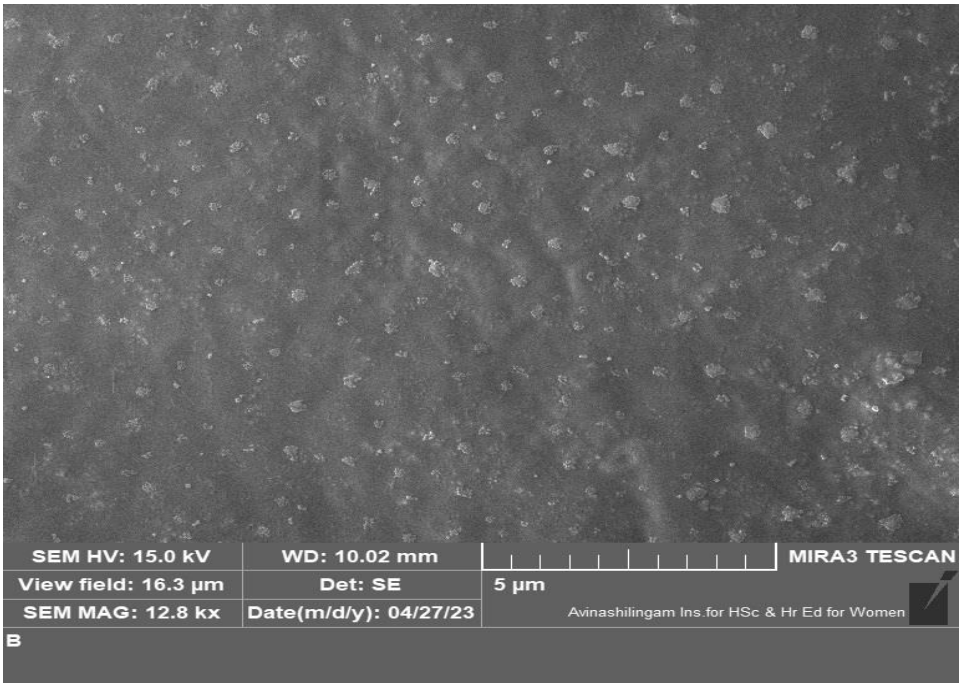

b) Scanning Electron Micrograph of 0.5% SCMC-ONB

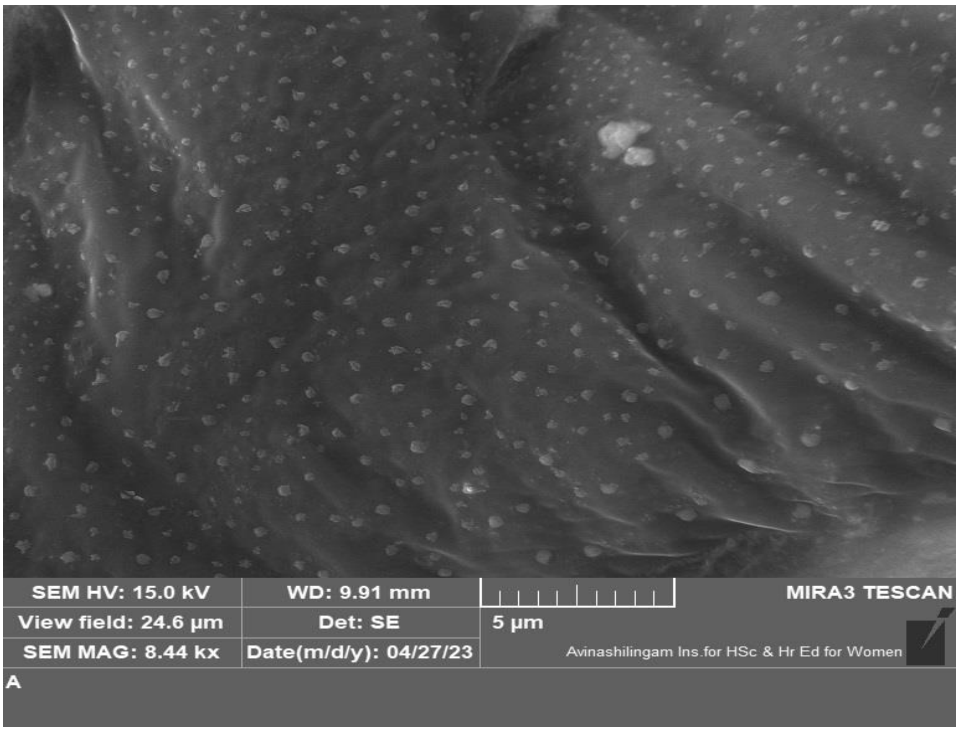

The distribution range of ONBs prepared by Khan *et al*. (2019) were mostly between 200 and 500 nm, with a mean size of about 300 nm. In the present study, the sizes were much smaller.

4.2.4 Energy Dispersive X-Ray Spectroscopy

The EDX analysis provides the elemental composition of the sample. The EDX result for 0.25% and 0.5% SCMC nanobubbles is shown in Figures 7 and 8 and Tables 8 and 9.

Figure 7

EDAX graph of 0.25% SCMC Nanobubbles

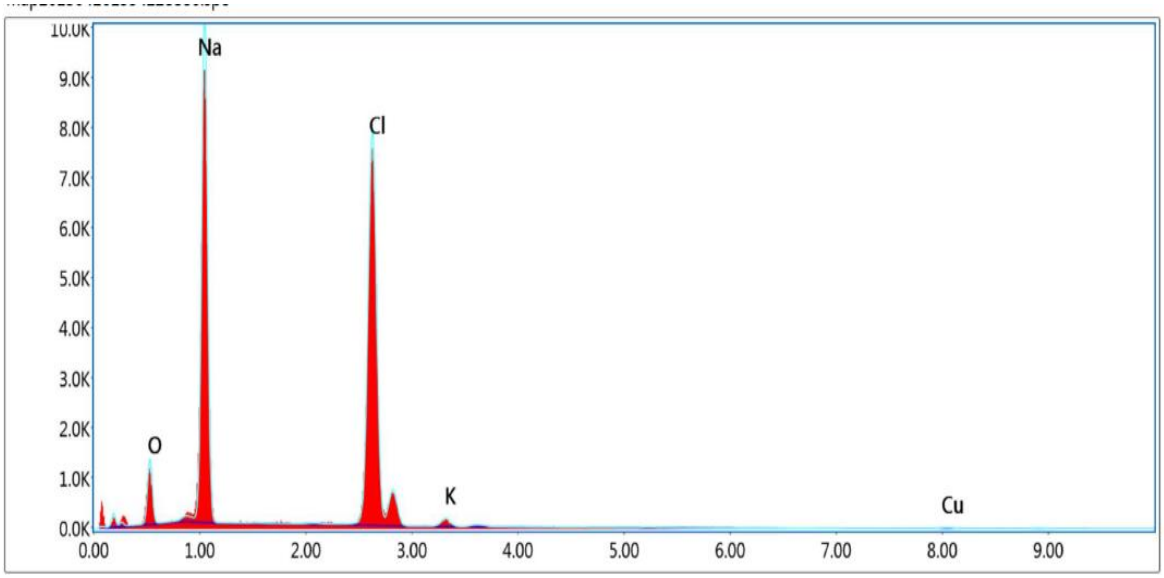

Table 8

EDAX Distribution of Elements in 0.25% SCMC nanobubbles

Element	Weight (%)	Atomic (%)	Net Int.	Error (%)	K ratio	Z	A	F
O	9.580	15.97	87.36	10.36	0.0256	1.1354	0.2357	1.0000
Na	40.42	46.92	838.6	5.130	0.2719	1.0274	0.654	1.0012
Cl	47.22	35.54	942.2	2.480	0.4197	0.9525	0.9314	1.0021
K	1.510	1.030	21.03	11.85	0.0122	0.9461	0.8476	1.0043
Cu	1.270	0.530	3.70	26.67	0.0111	0.8058	0.9987	1.0935

In the 0.25% & 0.5% SCMC ONBs, the sodium and chlorine levels were found to be almost similar while the level of oxygen was much less when compared to the sodium and chlorine levels. 0.5% SCMC ONB has 12 % of oxygen whereas 0.25% SCMC ONB has only 6% of oxygen. There were also traces of phosphorus (2%) and potassium (2%) in the nanobubbles due to the PBS used.

Figure 8

EDAX Distribution of Elements in 0.5% SCMC Nanobubbles

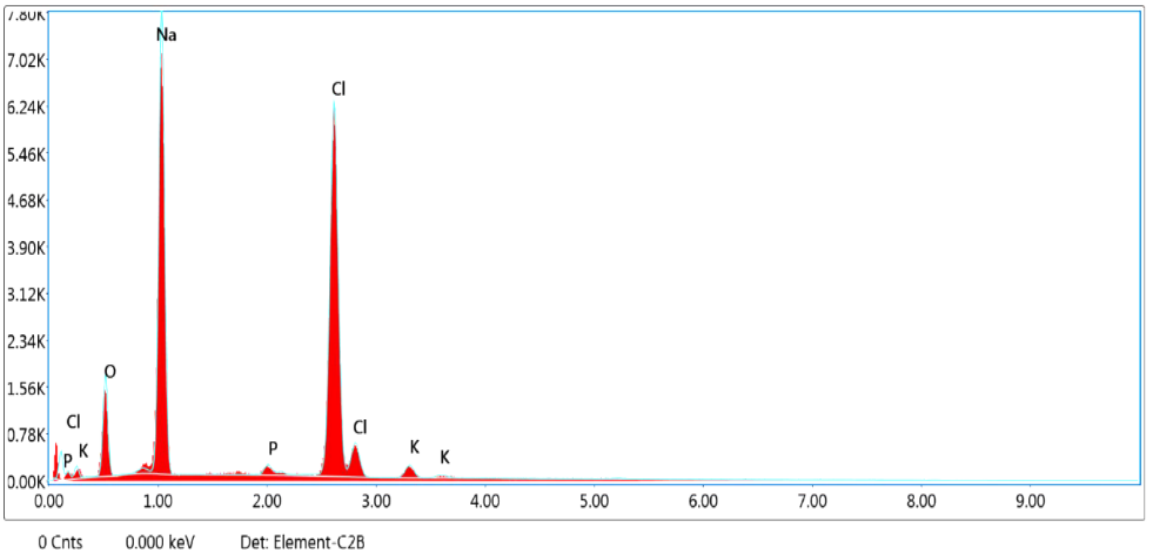

Table 9

EDX distribution of elements in 0.5% SCMC nanobubbles

Element	Weight (%)	Atomic (%)	Net Int.	Error (%)	K ratio	Z	A	F
O	11.67	19.12	74.25	10.47	0.0310	1.1304	0.2348	1.0000
Na	38.98	44.46	569.9	5.200	0.2627	1.0228	0.6580	1.0013
P	0.820	0.700	12.88	17.39	0.0068	0.9793	0.8335	1.0149
Cl	46.09	34.09	645.2	2.540	0.4085	0.9481	0.9326	1.0025
K	2.450	1.640	23.88	9.860	0.0197	0.9417	0.8510	1.0039

Kumar *et al*. (2020), analysed CMC and derivatives of CMC for nano porous hydrogel beads using EDX. The elemental composition was Carbon, Oxygen and Sodium with 45.95%, 32.48% and 21.57% by weight respectively. Oxygen content of ONBs of the present study were much lesser different in the present study.

In both samples, sodium and chlorine content is much larger than any other element, as they both are part of 0.1 M PBS solution. Oxygen content is the third highest percent in both samples by weight. Among the prepared ONBs, 0.5 % SCMC ONB was found to have higher

concentration of oxygen by weight. Based on both dissolved oxygen levels and EDX results, for further studies, 0.5 % SCMC ONB was selected for further studies.

4.2.5 Fourier Transform Infrared Spectroscopy

The Fourier Transform Infrared Spectrum of the 0.5% SCMC nanobubbles is given in Figure 9.

Figure 9

IR Spectrum of 0.5% SCMC Nanobubbles

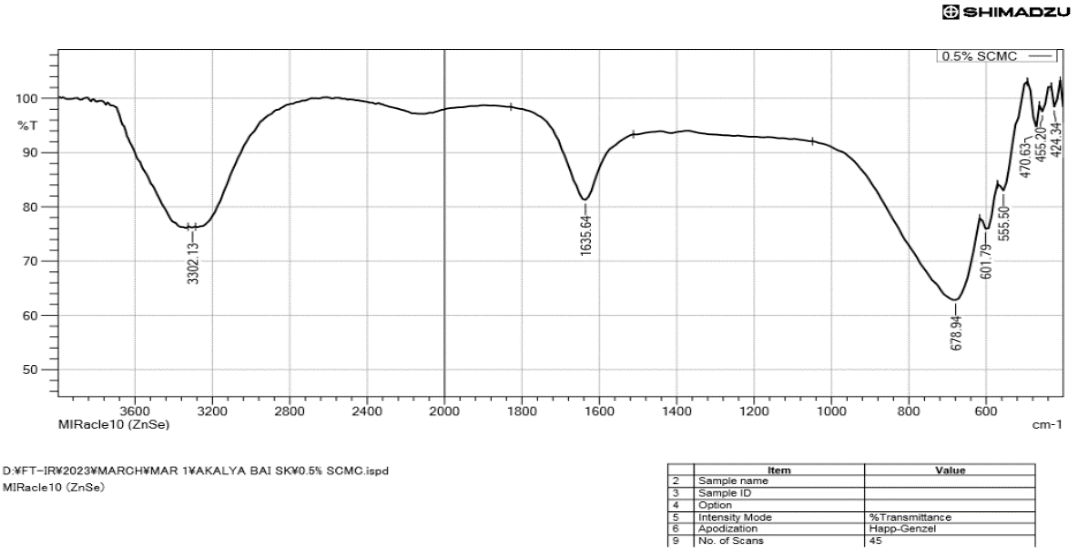

	Item	Value
2	Sample name	
3	Sample ID	
4	Option	
5	Intensity Mode	%Transmittance
6	Apodization	Happ-Genzel
9	No. of Scans	45

FTIR spectrum of 0.5% SCMC nanobubbles has three major peaks. First peak is at 3302.13 cm^{-1} corresponds to hydroxyl bond and C-H stretching bond of alkyne groups, second peak at 1635.54 cm^{-1} corresponds to C-H bond mainly present in aromatic compound as well to C-C bond in alkene and third peak is at 678.94 cm^{-1} corresponding to C-C bond of alkene group. Other small peaks are seen in following wavelengths: 601.79 $cm^{-}1$ indicates alcohol, OH out-of-plane bend, 555.5 cm^{-1} indicates aliphatic iodo compounds, C-I stretch, 470.63 cm^{-1},455.2 cm^{-1} and 424.34 cm^{-1} are related to fingerprint region.

Herrero *et al*. (2021) characterised Carboxymethyl Cellulose (CMC) by FTIR analysis. In their spectrum, the O-H stretching vibrations band appears at 3315 cm^{-1} in the CMC spectrum,

whereas the C-H stretching vibrations of the CH_2 groups are responsible for the band at 2918 cm^{-1}. The stretching vibrations of carboxylic and C-O groups are represented by the bands at 1620 and 1372 cm^{-1}.

Carboxymethyl Cellulose Sodium Alginate combination was characterised using FTIR analysis by Salama *et al*. (2019). In terms of intermolecular/intramolecular hydrogen-bonded OH stretching vibration, CMC/A film displayed a wide band at 3258 cm^{-1}. Both CMC and alginate showed symmetric and asymmetric COO stretching vibrations at 1606 cm^{-1} and 1412 cm^{-1}, respectively. The glycosidic connections in CMC and alginate are responsible for the high absorption band at 1023 cm^{-1}.

The FTIR analysis confirmed the presence of functional groups such as hydroxyl group, alkene and alkyne at different frequencies. All these functional groups are part of the sodium carboxymethyl cellulose which formed the major part of the nanobubbles prepared.

4.2.6 Three-Dimensional Optical Profiler

Three-dimensional optical profiler result depicts the surface height and surface roughness of 0.5% SCMC nanobubbles as shown in Figures 10a, 10b respectively and Figure 10c depicts the cross section of the nanobubbles.

Figure 10

Surface Morphology of 0.5% SCMC-ONB

a) Surface area of 0.5% SCMC nanobubbles

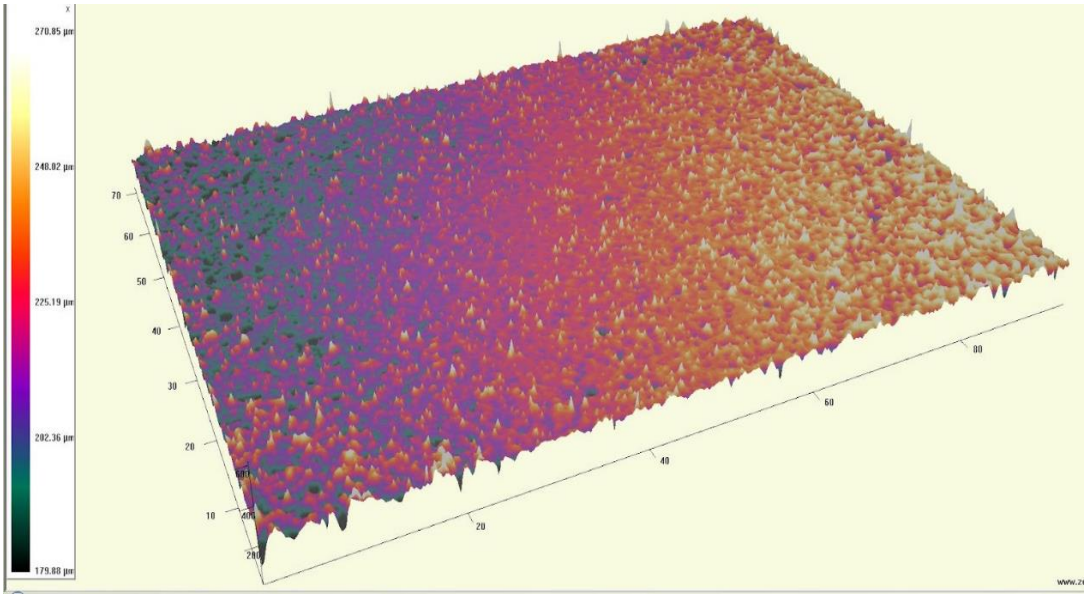

b) Cross section of the surface of 0.5% SCMC nanobubbles

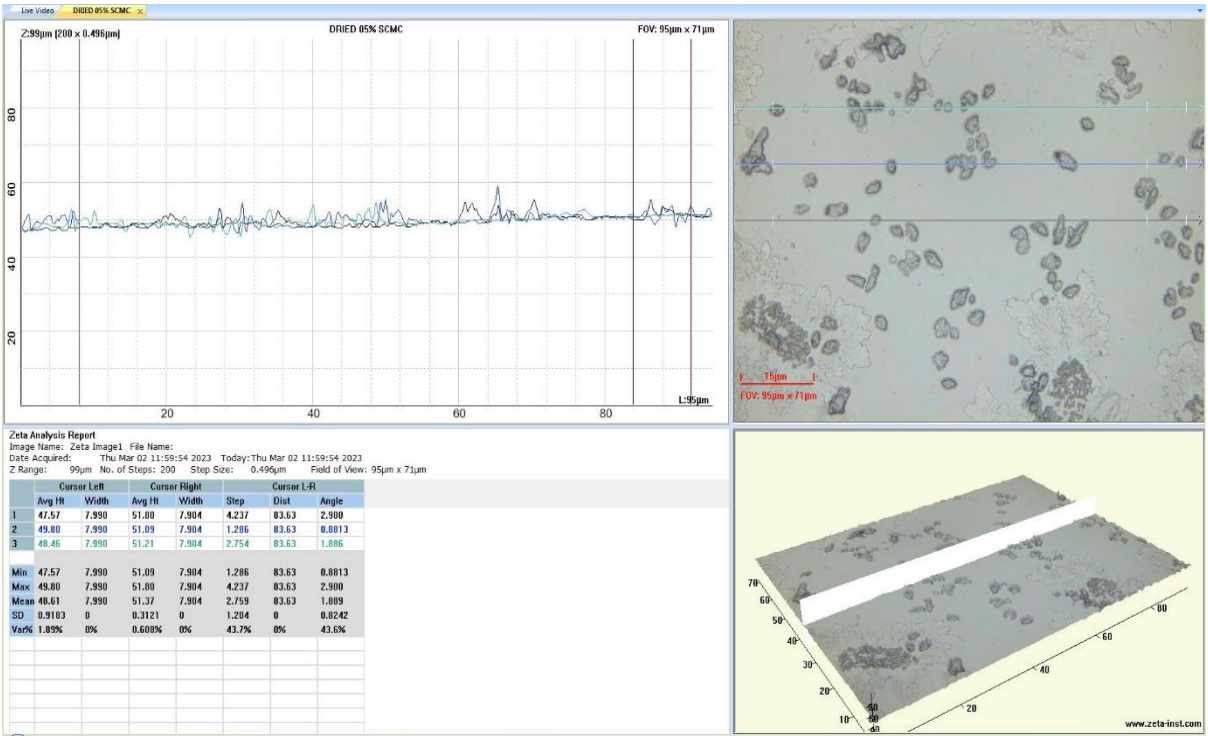

	Cursor Left		Cursor Right		Cursor L-R		
	Avg Ht	Width	Avg Ht	Width	Step	Dist	Angle
1	47.57	7.990	51.80	7.904	4.237	83.63	2.900
2	49.80	7.990	51.09	7.904	1.286	83.63	0.8813
3	48.46	7.990	51.21	7.904	2.754	83.63	1.886
Min	47.57	7.990	51.09	7.904	1.286	83.63	0.8813
Max	49.80	7.990	51.80	7.904	4.237	83.63	2.900
Mean	48.61	7.990	51.37	7.904	2.759	83.63	1.889
SD	0.9183	0	0.3121	0	1.204	0	0.8242
Var%	1.89%	0%	0.608%	0%	43.7%	0%	43.6%

c) **Height of the surface of 0.5% SCMC nanobubbles**

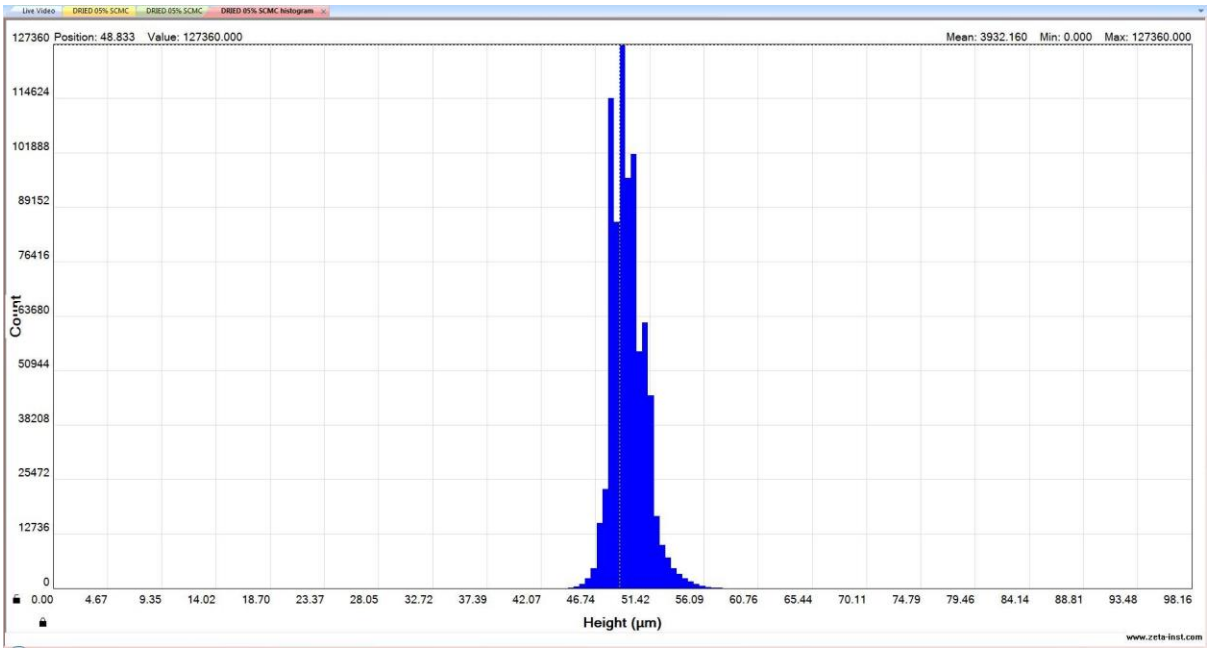

From the results of the three-dimensional optical profiler, we can infer that the 0.5% SCMC nanobubbles have a rough surface area. Figure 8a depicts the surface area roughness of the nanobubbles. Figure 8b displays the multiple cross section of the surface which follows an irregular pattern. Figure 8c showed a decreased but wide surface height for the nanobubbles in the range of 46 – 60 µm.

4.2.7 Transmission Electron Microscope

The TEM analysis infers the 3D structure, morphology and size of the SCMC ONB analysed and the result obtained for 0.5% SCMC nanobubbles is depicted in Figure 11. The morphology of the 0.5% SCMC nanobubbles is spherical in shape with a diameter ranging from 100 – 300 nm. The nanobubbles produced are distinct and dispersed evenly in the solution.

Zhang *et al*. (2020) also reported that the produced nanobubbles were spherical in form and had a high degree of structural stability at 25°C even after 24 h without changing in size or form.

Figure 11

TEM Image of 0.5% SCMC-ONB

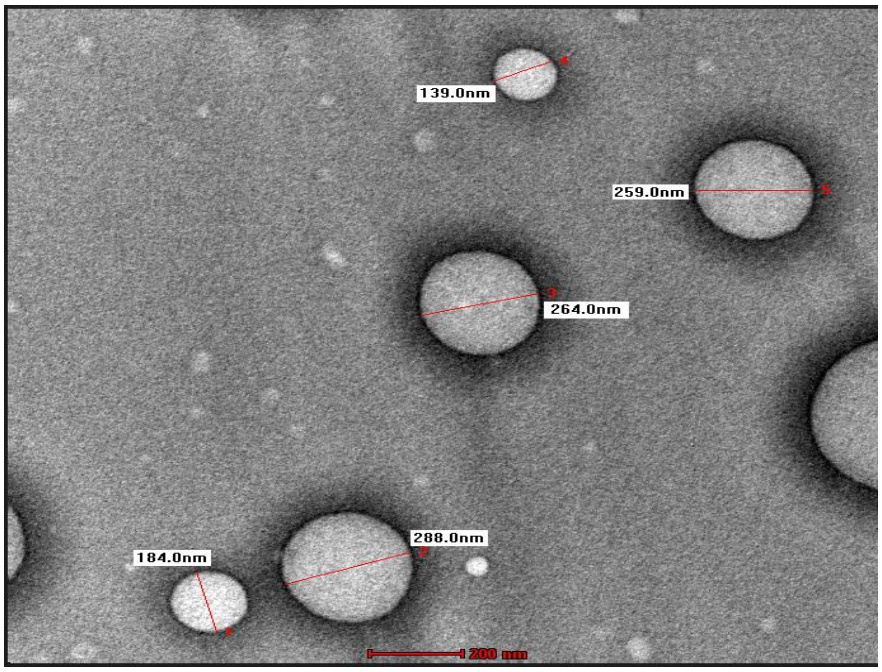

4.2.8 Absorption spectroscopy

The absorption spectra analysed to measure the absorption, the result for 0.5% SCMC nanobubbles is shown in Figure 12. The optical density stated that absorbance of the oxygen nanobubble sample is found to be highest at the wavelength of 250 nm in the UV range and steeply declined at higher wavelengths.

Figure 12

Absorption Spectra Graph of 0.5% SCMC-ONB

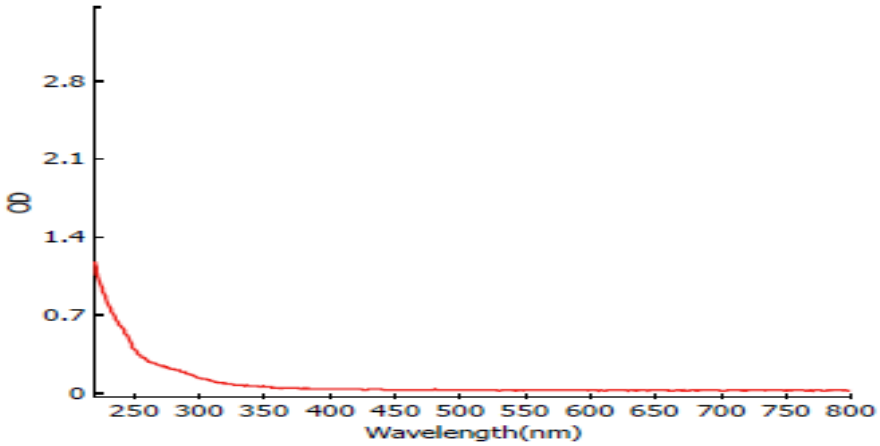

4.3 Animal Studies

Sodium Carboxymethyl Cellulose was used as shell material in various combinations to produce oxygen nanobubbles. Upon characterisation for nanobubble size, surface roughness, purity and oxygen releasing capacity 0.5% SCMC nanobubbles was selected to study their ability to reverse acute hypoxia in albino rats.

4.3.1 Oxygen Saturation

Pulse oximetry helps in determining the oxygen saturation in blood. Oxygen saturation in rats were monitored during experimental studies for a period of one hour. The mean oxygen levels of the rats of the different experimental groups are plotted in the graph shown in Figure 13 and Table 10.

Figure 13

Oxygen Saturation Graph

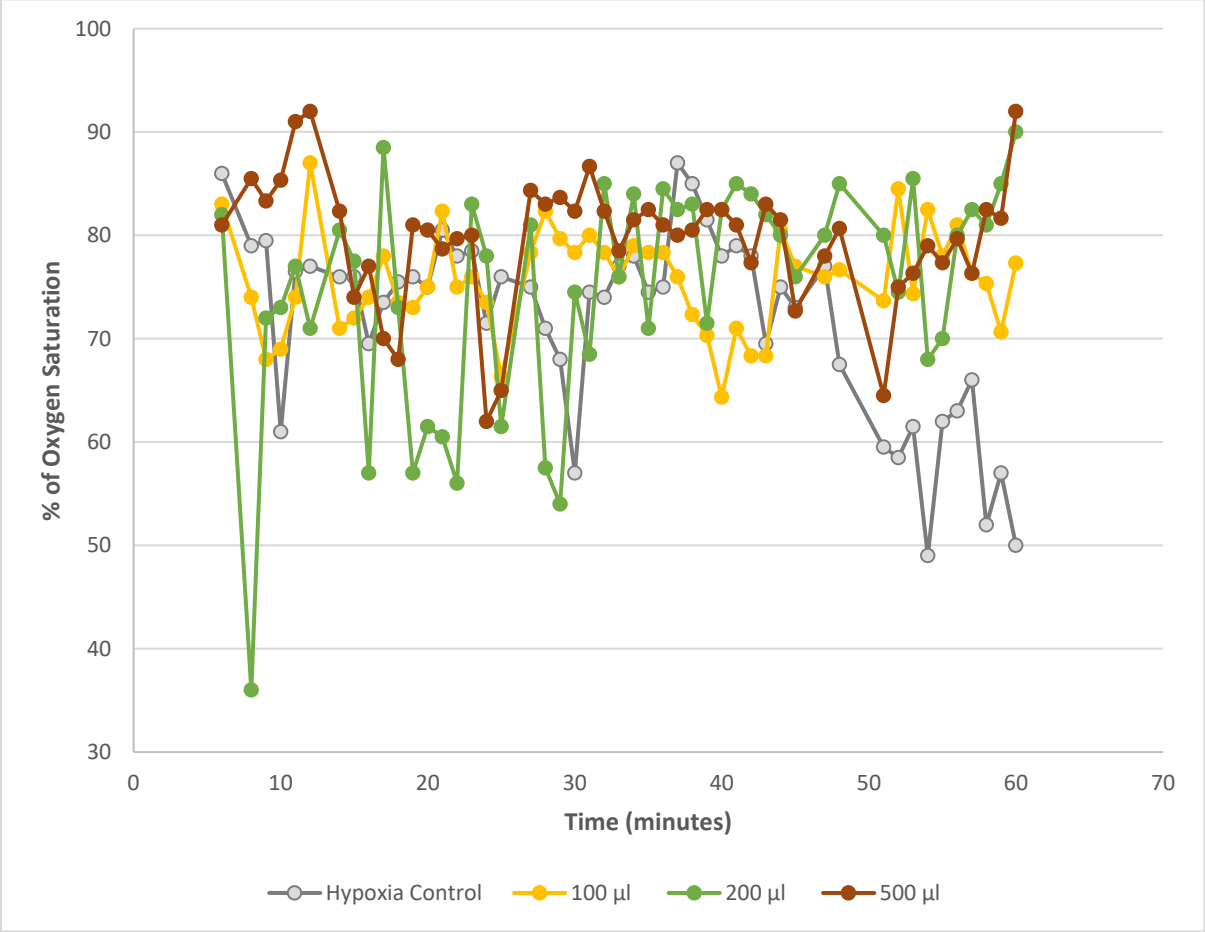

Table 10

Oxygen Saturation

Duration (minutes)	Group 1 (n = 3)	Group 2 (n = 3)	Group 3 (n = 3)	Group 4 (n = 3)	P Value
5	79.5 ± 1.5	68.6 ± 4.2	72.0 ±14	83.3 ± 10	0.239
10	61.0 ± 16	69.3 ± 2.1	75.0 ± 3.5	85.3 ± 9.0	0.095
15	76.0 ± 2.0	71.3 ± 1.2	77.5 ± 13	79.6 ± 8.2	0.623
20	74.5 ± 0.5	77.0 ± 3.5	61.5 ±15	80.6 ± 4.5	0.014*
25	76.0 ± 2.0	66.3 ± 17	61.5 ± 9.5	67.6 ± 9.3	0.469
30	57.0 ± 15	78.3 ± 5.1	74.5 ± 0.5	82.3 ± 11	0.052
35	74.5 ± 1.5	78.3 ± 5.9	78.0 ± 12	85.0 ± 7.0	0.439
40	81.5 ± 6.5	64.3 ± 25	82.5 ± 7.5	78.0 ± 12	0.449
45	69.5 ± 0.5	75.6 ± 4.6	76.0 ± 2.0	72.0 ± 21	0.862
50	59.5 ± 12	73.0 ± 8.2	80.5 ± 11	74.6 ± 13	0.211
55	62.0 ± 17	74.3 ± 8.1	76.3 ± 11	77.3 ± 13	0.467
60	66.0 ± 5.0	77.3 ± 11	83.6 ± 11	86.3 ± 11	0.132

Group 1 – Hypoxia Control; Group 2 – hypoxia + 100 µl SCMC ONB treatment; Group 3 – hypoxia + 200 µl SCMC ONB treatment; Group 4 – hypoxia + 500 µl SCMC ONB treatment * $p < 0.05$

The oxygen saturation in 500 µl treatment group is higher than any other experimental group. The highest oxygen saturation range attained in 500 µl treatment group was 90 – 95% at 12^{th} and 60^{th} minutes. Significant increase in oxygen saturation was observed at 20 minutes ($p = 0.014$) in rats administered with 500 µl SCMC ONB. Even though, no significance was observed at other time points, a general high O_2 saturation was observed in SCMC-ONB treated groups.

Inglin *et al*. (2019) mixed commercial Vicryl sutures with the CPO-PLGA combination in an effort to create a surgical material that allows oxygen to be applied directly to the anastomosis.

The impact of this oxygen-producing suture material on the healing of colorectal anastomoses was evaluated *in vivo* using an experimental model. There was no statistically significant difference between the different treatment groups with respect to baseline or immediate postoperative values. StO2 was significantly higher for PLGA–CPO than for Vicryl or PLGA anastomoses. The present study results are different from those obtained by Inglin *et al*. (2019).

4.3.1 Biochemical Studies

4.3.1.1 Acute phase proteins

Acute-phase proteins are a group of proteins whose blood plasma concentrations either rise in response to inflammation (positive acute-phase proteins) or fall (negative acute-phase proteins).

4.3.1.1.1 C - Reactive Protein Levels

C – Reactive Protein (CRP) is a positive acute-phase protein and thus they rise in blood levels upon inflammation. The study is conducted to analyse the relation between CRP levels and hypoxic condition in rats. C-Reactive protein assay is used to determine the inflammatory level in rats. The results are tabulated in Table 11.

Table 11

CRP levels

Group	Mean ± SD (mg/dl)	P value
Group 1 (G1)	43.0 ± 6.35	
Group 2 (G2)	40.6 ± 8.24	G2 vs G1 - 0.682 G2 vs G3 - 0.177 G2 vs G4 - 0.103
Group 3 (G3)	29.4 ± 8.59	G3 vs G1 - 0.071 G3 vs G4 - 0.829
Group 4 (G4)	30.5 ± 0.96	G4 vs G1 - 0.009*

Group 1 – Hypoxia Control; Group 2 – hypoxia + 100 µl SCMC ONB treatment; Group 3 – hypoxia + 200 µl SCMC ONB treatment; Group 4 – hypoxia + 500 µl SCMC ONB treatment * $p < 0.05$

Guo *et al*. (2015) investigated the impact of tempol on endothelial cell apoptosis signals and the influence of lymphocytes from intermittent hypoxia exposed rats. The results of the study

showed that the level of CRP had significantly risen. CRP has been shown to induce endothelial apoptosis.

Sheriif *et al*. (2021) reported that High CRP concentrations during the first 48 h after the acute myocardial infarction incident significantly predict immediate and long-term mortality as well as the overall prognosis.

Unpaired Student's T test was performed and CRP levels of group 4 (500 µl SCMC-ONB treated) rats were significantly lesser than that of hypoxia control group. This indicates that administration of 500 µl SCMC-ONBs are able to reverse the inflammatory condition induced by hypoxia. This implies that SCMC-ONB has significant impact on decreasing the levels of acute phase protein, CRP.

4.3.1.2 Blood coagulation proteins

D-Dimer and fibrinogen proteins are involved in blood coagulation. D-Dimer is a degradation product of fibrin and fibrinogen gets converted to fibrin, which is base for blood coagulation. The animals under hypoxic condition might have cell damage and tissue damage in them. Damage in tissues or cells can increase the level of these protein levels in blood, thus analysis was done to identify their relation to these parameters.

4.3.1.2.1 Fibrinogen Levels

Fibrinogen assay is used to determine the blood clotting condition in rats. Unpaired T Test was done and significant difference was observed between hypoxia control and oxygen nanobubble treatment groups.

Table 12

Fibrinogen levels

Group	Mean ± SD (mg/dl)	P Value
Group 1 (G1)	45.26 ± 5.21	
Group 2 (G2)	31.41 ± 3.88	G2 vs G1 - 0.005** G2 vs G3 - 0.236 G2 vs G4 - 0.339
Group 3 (G3)	26.35 ± 2.33	G3 vs G1 - 0.007* G3 vs G4 - 0.609
Group 4 (G4)	22.76 ± 5.25	G4 vs G1 - 0.004**

Group 1 – Hypoxia Control; Group 2 – hypoxia + 100 µl SCMC ONB treatment; Group 3 – hypoxia + 200 µl SCMC ONB treatment; Group 4 – hypoxia + 500 µl SCMC ONB treatment * $p < 0.05$; ** $p < 0.005$

Ninivaggi *et al*. (2015) analysed the effects of hypobaric hypoxia exposure in venous thromboembolism. They reported that on exposure to hypobaric hypoxia, fibrinolysis and fibrinogen levels were not affected as well, blood thrombin generation in plasma also did not increase. So, they demonstrated that hypoxia causes a prothrombic state. The present study does not correlate with the study carried out by Ninivaggi *et al*. (2015), showing that SCMC – ONBs reduce the effect of hypoxia in blood coagulation.

4.3.1.2.2 D-Dimer Levels

D-Dimer assay is used to determine the blood clotting condition in rats. The results are tabulated in Table 13. Unpaired Student's T test was performed and reported no significant difference among the experimental groups. The SCMC-ONBs failed to reduce the fibrin degradation and thus results in high level of D-Dimer in serum.

Table 13

D-Dimer levels

Group	Mean ± SD (mg/dl)	P Value
Group 1 (G1)	130.8 ± 26.7	
Group 2 (G2)	106.7 ± 4.60	G2 vs G1 - 0.099 G2 vs G3 - 0.080 G2 vs G4 - 0.578
Group 3 (G3)	141.4 ± 39.4	G3 vs G1 - 0.696 G3 vs G4 - 0.210
Group 4 (G4)	126.8 ± 14.1	G4 vs G1 - 0.789

Group 1 – Hypoxia Control; Group 2 – hypoxia + 100 µl SCMC ONB treatment; Group 3 – hypoxia + 200 µl SCMC ONB treatment; Group 4 – hypoxia + 500 µl SCMC ONB treatment * $p < 0.05$

Levkovsky *et al*. (2020) made an attempt to explore changes in parameters of coagulation and fibrinolysis in rat models of exposure to hypoxia and hypobaric hypoxia during travel. They reported that no effect of various exposure conditions was observed on D-Dimer, Interleukin – 1, Interleukin – 6, blood count and thrombin – antithrombin complex for two and twelve hours of exposure. This strongly supports the present study for no significant difference in one hour of exposure to hypoxic conditions.

5.0 SUMMARY AND CONCLUSION

Acute hypoxia may be due to low levels of oxygen or low levels of partial pressure of oxygen in an organism. People with prolonged cardiac and respiratory problem are under major risk for hypoxia. It may be the root cause of several diseases like cancer, cardiovascular diseases and neurodegenerative diseases. The present study was undertaken to synthesise oxygen nanobubbles and assessing their ability to reverse acute hypoxia in rats.

Oxygen nanobubbles (ONB) are carriers of oxygen which are designed to deliver them to the required tissues. They will have a hydrophilic shell layer and a core region containing gas. In present study, nanobubbles were prepared with sodium carboxymethyl cellulose (SCMC) as shell material. After trying various combinations of concentrations of SCMC and aqueous solutions, the promising combinations of 0.25% and 0.5% SCMC and 0.1 M phosphate buffered saline (pH 7.4) as aqueous solution were used to prepare nanobubbles. This combination was selected by determining the diameter size, polydispersity index and zeta potential of the prepared nanobubbles. The prepared nanobubbles had diameter in the range of 50 -300 nm.

Dissolved oxygen content of nanobubbles were determined to assess the oxygen carrying capacity of them. Among 0.25% and 0.5% SCMC ONB, the latter led to an increase of about 30 – 35% of oxygen content in a degassed solution. From the images of FESEM, both nanobubbles were spherical in shape and from EDX results, it was inferred that 0.5% SCMC ONB had higher oxygen content than 0.25% SCMC ONB. So, for further studies 0.5% SCMC ONB was used.

0.5% SCMC ONB was further characterised to identify their elemental composition, surface roughness, surface height and 3D structure. IR spectrum revealed that the nanobubbles had hydroxyl group, C – H stretch of alkyne group, C – C bone of alkenes, C – H bonds of aromatic compounds and very low levels of aliphatic iodo compounds were present. Three-Dimensional optical profiler results showed that the shell layer of nanobubbles is of rough surface and has a surface height of 46 -60 µm. TEM analysis confirmed that the nanobubbles are spherical in shape and in the range of 50 – 300 nm.

Animal studies were carried out in Wistar albino rats of 200 -250 g weight. The rats were grouped into 4 groups containing a hypoxia control group and all the other three were nanobubble

treatment groups. 100 µl, 200 µl and 500 µl of 0.5% SCMC ONB are the dosage for treatment groups. Hypoxia was induced by administering ketamine hydrochloride in rats and after 10 minutes of ketamine administration, nanobubbles were given intravenously, as treatment to reverse the induced hypoxic condition. Oxygen saturation of rats was assessed for one hour after ketamine administration at frequent intervals. Results for oxygen saturation in rats inferred the significant relation between the nanobubble treatment groups ($p < 0.05$).

At the end of one hour of experiment, blood was drawn from the rats through heart puncture and assessed the levels of C – Reactive protein (CRP), and coagulation proteins, D - Dimer and fibrinogen. On conducting Unpaired T Test, significant reduction in levels of CRP and fibrinogen was observed. No effective impact was seen in D-Dimer levels.

In conclusion, 0.5% SCMC ONB prepared using 0.1 M PBS as aqueous solution was effective in reversing hypoxia by increasing the oxygen saturation and reducing the levels of CRP and fibrinogen in blood. Measures have to be taken to improvise the nanobubble preparation and in reversing tissue hypoxia.

6.0 BIBLIOGRAPHY

A. d. Leon, R. Perera, P. Nittayacharn, M. Cooley, O. Jung and A. A. Exner, Ultrasound contrast agents and delivery systems in cancer detection and therapy, Adv. Canc. Res., 2018, 139, 57–84.

A. Exner and M. C. Kolios, Bursting microbubbles: how nanobubble contrast agents can enable the future of medical ultrasound molecular imaging and image-guided therapy, Curr. Opin. Colloid Interface Sci., 2021, 54, 101463.

A. Oishi, H. Shimokawa, E. Sakaniwa, M. Takahashi, M. Miyashin and S. Arakawa, Oxygen and air nanobubbles in water inhibit proliferation of dental follicle stem cells in vitro, J. Dent. Health Oral Disord. Ther., 2018, 9(6), 460– 462.

A. S. Thakor and S. S. Gambhir, Nanooncology: the future of cancer diagnosis and therapy, Ca - Cancer J. Clin., 2013, 63(6), 395–418.

Adeel, M.; Duzagac, F.; Canzonieri, V.; Rizzolio, F. Self-therapeutic nanomaterials for cancer therapy: A review. ACS Appl. Nano Mater. **2020**, 3, 4962–4971. [CrossRef]

Argenziano, M., Occhipinti, S., Scomparin, A., Angelini, C., Novelli, F., Soster, M., Giovarelli, M., & Cavalli, R. (2022). Exploring chitosan-shelled nanobubbles to improve HER2 + immunotherapy via dendritic cell targeting. Drug Delivery and Translational Research, 12(8), 2007–2018. https://doi.org/10.1007/s13346-022-01185-8

Ashizawa K. (2019). Yakugaku zasshi: Journal of the Pharmaceutical Society of Japan, 139(2), 237-248. https://doi.org/10.1248/yakushi. 18- 00171-1

Bach J. (2017). A Quick Reference on Hypoxemia. *The Veterinary clinics of North America. Small animal practice*, *47*(2), 175–179. https://doi.org/10.1016/j.cvsm.2016.10.004

Banche, G., Allizond, V., Mandras, N., Finesso, N., Luganini, A., Genova, T., Argenziano, M., Magnetto, C., Gulino, G. R., Roana, J., Tullio, V., Giribaldi, G., Cavalli, R., Spagnolo, R., Troia, A., Cuffini, A. M., & Prato, M. (2022). Antimicrobial oxygen-loaded nanobubbles as promising tools to promote wound healing in hypoxic human keratinocytes. *Toxicology reports*, *9*, 154–162. https://doi.org/10.1016/j.toxrep.2022.01.005

Bao, M. H., & Wong, C. C. (2021). Hypoxia, Metabolic Reprogramming, and Drug Resistance in Liver Cancer. *Cells*, *10*(7), 1715. https://doi.org/10.3390/cells10071715

Bayda, S., Adeel, M., Tuccinardi, T., Cordani, M., & Rizzolio, F. (2019). The History of Nanoscience and Nanotechnology: From Chemical-Physical Applications to

Nanomedicine. *Molecules (Basel, Switzerland)*, *25*(1), 112. https://doi.org/10.3390/molecules25010112

Becerril,M. A., Aranda-Lara, L., Isaac-Olivé, K., Ocampo-García, B. E., & Morales-Ávila, E. (2022). Nanocarriers for delivery of siRNA as gene silencing mediator. *EXCLI journal*, *21*, 1028–1052. https://doi.org/10.17179/excli2022-4975

Bekos, C., Grimm, C., Brodowicz, T., Petru, E., Hefler, L., Reimer, D., ... & Polterauer, M. (2017). Prognostic role of plasma fibrinogen in patients with uterine leiomyosarcoma–a multicenter study. *Scientific Reports*, *7*(1), 1-7.

Bhandari, P.; Wang, X.; Irudayaraj, J. Oxygen nanobubble tracking by light scattering in single cells and tissues. ACS Nano **2017**, 11, 2682–2688. [CrossRef] [PubMed]

Bhandari, P.N.; Cui, Y.; Elzey, B.D.; Goergen, C.J.; Long, C.M.; Irudayaraj, J. Oxygen nanobubbles revert hypoxia by methylation programming. Sci. Rep. **2017**, 7, 9268. [CrossRef] [PubMed]

Bhutta, B.S.; Alghoula, F.; Berim, I. (9 August 2022). "Hypoxia". Treasure Island, FL: StatPearls [Internet]. PMID 29493941.

Boysen SR, Lisciandro GR. The use of ultrasound for dogs and cats in the emergency

Burtscher, J., Mallet, R. T., Burtscher, M., & Millet, G. P. (2021). Hypoxia and brain aging: Neurodegeneration or neuroprotection? *Ageing research reviews*, *68*, 101343. https://doi.org/10.1016/j.arr.2021.101343

C. Kim, R. Qin, J. S. Xu, L. V. Wang and R. Xu, Multifunctional microbubbles and nanobubbles for photoacoustic and ultrasound imaging, Biomed. Opt., 2015, 15, 13–15.

Calgaroto, S., Wilberg, K., & Rubio, J. A. (2014b). On the nanobubbles interfacial properties and future applications in flotation. Minerals Engineering, 60, 33–40. https://doi.org/10.1016/j.mineng.2014.02.002

Cavalli, R., Bisazza, A., Rolfo, A., Balbis, S., Madonnaripa, D., Caniggia, I., & Guiot, C. (2009). Ultrasound-mediated oxygen delivery from chitosan nanobubbles. *International journal of pharmaceutics*, *378*(1-2), 215–217. https://doi.org/10.1016/j.ijpharm.2009.05.058

Cavalli, R., Soster, M., & Argenziano, M. (2016). Nanobubbles: a promising efficient tool for therapeutic delivery. Therapeutic delivery, 7(2), 117–138. https://doi.org/10.4155/tde.15.92

Cavalli, R.; Bisazza, A.; Lembo, D. Micro-and nanobubbles: A versatile non-viral platform for gene delivery. Int. J. Pharm. **2013**, 456, 437–445. [CrossRef] [PubMed]

Cavalli, R.; Soster, M.; Argenziano, M. Nanobubbles: A promising efficienft tool for therapeutic delivery. Ther. Deliv. **2016**, 7, 117–138. [CrossRef] [PubMed]

Choudhury R. (2018). Hypoxia and hyperbaric oxygen therapy: a review. *International journal of general medicine, 11*, 431–442. https://doi.org/10.2147/IJGM.S172460

Chris, Melitus & Wilkesa, Kimberly. (2019). The Crucial Role of Oxygen for Health. Journal of Restorative Medicine. 8. 10.14200/jrm.2019.0106.

Comellini, V., Pacilli, A. M. G., & Nava, S. (2019). Benefits of non-invasive ventilation in acute hypercapnic respiratory failure. *Respirology (Carlton, Vic.), 24*(4), 308–317. https://doi.org/10.1111/resp.13469

Cyanobacteria. *The New phytologist*, *225*(4), 1440–1446. https://doi.org/10.1111/nph.16249
D. V. B. Batchelor, F. J. Armistead, N. Ingram, S. A. Peyman, J. R. Mclaughlan, P. L. Coletta, et al., Nanobubbles for therapeutic delivery: production, stability and current prospects, Curr. Opin. Colloid Interface Sci., 2021, 54, 101456.

DeCoste, J.B.;Weston, M.H.; Fuller, P.E.; Tovar, T.M.; Peterson, G.W.; LeVan, M.D.; Farha, O.K. Metal-organic frameworks for oxygen storage. Angew. Chem. Int. Edit. **2014**, 53, 14092–14095. [CrossRef]

Dixon, A.J.; Hu, S.; Klibanov, A.L.; Hossack, J.A. Oscillatory dynamics and in vivo photoacoustic imaging performance of plasmonic nanoparticle-coated microbubbles. Small **2015**, 11, 3066–3077. [CrossRef] [PubMed]

Dominguez-Martin, M. A., Hammel, M., Gupta, S., Lechno-Yossef, S., Sutter, M., Rosenberg, D. W., Chen, Y., Petzold, C. J., Ralston, C. Y., Polívka, T., & Kerfeld, C. A. (2020). Structural analysis of a new carotenoid-binding protein: the C-terminal domain homolog of the OCP. Scientific Reports, 10(1). https://doi.org/10.1038/s41598-020-72383-y
Dong F, Zhang J, Wang K, Liu Z, Guo J, Zhang J (2019) Correction: cold plasma gas loaded microbubbles as a novel ultrasound contrast agent. Nanoscale 11:1123–1130

Drake M. G. (2018). High-Flow Nasal Cannula Oxygen in Adults: An Evidence-based Assessment. *Annals of the American Thoracic Society*, *15*(2), 145–155. https://doi.org/10.1513/AnnalsATS.201707-548FR

E. M. Knavel and C. L. Brace, Tumor ablation: common modalities and general practices, Tech. Vasc. Interv. Radiol., 2013, 16(4), 192–200.
E. P. Favvas, G. Z. Kyzas, E. K. E□himiadou and A. C. Mitropoulos, Bulk nanobubbles, generation methods and potential applications, Curr. Opin. Colloid Interface Sci., 2021, 54, 101455.

F. Conversano, R. Franchini, A. Lay-ekuakille and S. Casciaro, In vitro evaluation and theoretical modelling of the dissolution behavior of a microbubble contrast agent for ultrasound imaging, IEEE Sens. J., 2012, 12(3), 496–503.

F. J. Rodera, M. J. Moore, Y. Wang, A. C. D. Leon, E. Abenojar, A. A. Exner, et al., Nanobubble facilitated optoporation and photoacoustic imaging of BT-474 breast cancer cells, IEEE Int. Ultrason. Symp., 2018, 1–4.

Fang J, Nakamura H, Maeda H. The EPR effect: unique features of tumor blood vessels for drug delivery, factors involved, and limitations and augmentation of the effect. *Adv. Drug Del. Rev.* 63(3), 136–151 (2011).

Farkas, N., & Kramar, J. A. (2021c). Dynamic light scattering distributions by any means. Journal of Nanoparticle Research, 23(5). https://doi.org/10.1007/s11051-021-05220-6

Fix, S.M.; Borden, M.A.; Dayton, P.A. Therapeutic gas delivery via microbubbles and liposomes. J. Control. Release **2015**, 209, 139–149. [CrossRef] [PubMed]

Fokong S, Theek B, Wu Z *et al.* Image-guided, targeted and triggered drug delivery to tumors using polymer-based microbubbles. *J. Control. Rel.* 163, 75–81 (2012).

Gao, S.T.; Zheng, P.L.; Li, Z.H.; Feng, X.C.; Yan, W.X.; Chen, S.Z.; Guo, W.S.; Liu, D.D.; Yang, X.J.; Wang, S.X.; et al. Biomimetic O2-evolving metal-organic framework nanoplatform for highly efficient photodynamic therapy against hypoxic tumor. Biomaterials **2018**, 178, 83–94. [CrossRef]

Guarnizo-Herrero, V., Torrado-Salmerón, C., Torres Pabón, N. S., Torrado Durán, G., Morales, J., & Torrado-Santiago, S. (2021). Study of Different Chitosan/Sodium Carboxymethyl Cellulose Proportions in the Development of Polyelectrolyte Complexes for the Sustained Release of Clarithromycin from Matrix Tablets. *Polymers*, *13*(16), 2813. https://doi.org/10.3390/polym13162813

Guo, H., Cao, J., Li, J., Yang, X., Jiang, J., Feng, J., Li, S., Zhang, J., & Chen, B. (2015). Lymphocytes from intermittent hypoxia-exposed rats increase the apoptotic signals in endothelial

cells via oxidative and inflammatory injury in vitro. *Sleep & breathing = Schlaf & Atmung*, *19*(3), 969–976. https://doi.org/10.1007/s11325-015-1128-8

Gupta S, Donn SM. Continuous positive airway pressure: Physiology and comparison of devices. Semin Fetal Neonatal Med. 2016 Jun;21(3):204-11. [PubMed] [Reference list]

H. Y. Lee, H. Rhim, M. W. Lee, Y. Kim, D. Choi, M. J. Park, et al., Early diffuse recurrence of hepatocellular carcinoma a□er percutaneous radiofrequency ablation: analysis of risk factors, Eur. Radiol., 2013, 23(1), 190–197.

H. Yang, W. Cai, L. Xu, X. Lv, Y. Qiao, P. Li, et al., Nanobubble-Affibody: novel ultrasound contrast agents for targeted molecular ultrasound imaging of tumor, Biomaterials, 2015, 37, 279–28

Hadinger KP, Marshalek JP, Sheeran PS, Dayton PA, Matsunaga TO (2018) Optimization of phase-change contrast agents for targeting MDA-MB-231 breast cancer cells. Ultrasound Med Biol 44:2728–2738

Hamel J. A review of acute cyanide poisoning with a treatment update. Crit Care Nurse 2011;31(1):72-81.

Hirsh, Victor J. Marder, and Edwin W. Salzman. 1197 – 1206, J.B. Lippincott Company, 1994.

Hulla, J.; Sahu, S.; Hayes, A. Nanotechnology. Hum. Exp. Toxicol. **2015**, 34, 1318–1321. [CrossRef] [PubMed]

Huynh, E.; Jin, C.S.;Wilson, B.C.; Zheng, G. Aggregate enhanced trimodal porphyrin shell microbubbles for ultrasound, photoacoustic, and fluorescence imaging. Bioconjug. Chem. **2014**, 25, 796–801. [CrossRef] [PubMed]

Iijima, M.; Gombodorj, N.; Tachibana, Y.; Tachibana, K.; Yokobori, T.; Honma, K.; Nakano, T.; Asao, T.; Kuwahara, R.; Aoyama, K.; et al. Development of single nanometer-sized ultrafine oxygen bubbles to overcome the hypoxia-induced resistance to radiation therapy via the suppression of hypoxia-inducible factor-1. Int. J. Oncol. **2018**, 52, 679–686. [CrossRef] [PubMed]

Inglin, R. A., Brügger, L. E., Candinas, D., Harrison, B. S., & Eberli, D. (2019). Effect of oxygen-producing suture material on hypoxic colonic anastomoses in an experimental model. *BJS open*, *3*(6), 872–881. https://doi.org/10.1002/bjs5.50220

J. Liu, Y. Chen, G. Wang, Q. Lv, Y. Yang, J. Wang, et al., Biomaterials ultrasound molecular imaging of acute cardiac transplantation rejection using nanobubbles targeted to T lymphocytes, Biomaterials, 2018, 162, 200–207

Jackson, J. C., Mitchell, N., & Hopkins, R. O. (2015). Cognitive functioning, mental health, and quality of life in ICU survivors: an overview. *The Psychiatric clinics of North America*, *38*(1), 91–104. https://doi.org/10.1016/j.psc.2014.11.002

Jin, M. Lin, M. You, Y. Zong, M. Wan and F. Xu, Microbubble embedded with upconversion nanoparticles as a bimodal contrast agent for uorescence and ultrasound imaging, Nanotechnology, 2015, 26(34), 345601.

Kapłonek, W., Mikolajczyk, T., Pimenov, D. Y., Gupta, M. C., Mia, M., Sharma, S., Patra, K., & Sutowska, M. (2020b). High-Accuracy 3D Optical Profilometry for Analysis of Surface Condition of Modern Circulated Coins. Materials, 13(23), 5371. https://doi.org/10.3390/ma13235371

Khan, M. S., Hwang, J., Seo, Y., Shin, K., Lee, K., Park, C., Choi, Y., Hong, J. W., & Choi, J. (2018). Engineering oxygen nanobubbles for the effective reversal of hypoxia. *Artificial cells, nanomedicine, and biotechnology*, *46*(sup3), S318–S327. https://doi.org/10.1080/21691401.2018.1492420

Khan, M.S.; Hwang, J.; Lee, K.; Choi, Y.; Seo, Y.; Jeon, H.; Hong, J.W.; Choi, J. Anti-tumor drug-loaded oxygen nanobubbles for the degradation of HIF-1 alpha and the upregulation of reactive oxygen species in tumor cells. Cancers **2019**, 11, 17. [CrossRef] [PubMed]

Kheir, J.N.; Polizzotti, B.D.; Thomson, L.M.; O'Connell, D.W.; Black, K.J.; Lee, R.W.; Wilking, J.N.; Graham, A.C.; Bell, D.C.; McGowan, F.X. Bulk manufacture of concentrated oxygen gas-filled microparticles for intravenous oxygen delivery. Adv. Healthc. Mater. **2013**, 2, 1131–1141. [CrossRef] [PubMed]

Kheir, J.N.; Scharp, L.A.; Borden, M.A.; Swanson, E.J.; Loxley, A.; Reese, J.H.; Black, K.J.; Velazquez, L.A.; Thomson, L.M.;Walsh, B.K.; et al. Oxygen gas-filled microparticles provide intravenous oxygen delivery. Sci. Transl. Med. **2012**, 4, 140ra188. [CrossRef] [PubMed]

Klocke, R. A. , Cherniack, . Neil S. , Weibel, . Ewald R. , Heath, . Donald Albert , Elliott, . David H. , Siebens, . Arthur A. , Beers, . Michael F. and Burri, . Peter H. (2023, March 31). human respiratory system. Encyclopedia Britannica. https://www.britannica.com/science/human-respiratory-system

Koshiyama, K.;Wada, S. Collapse of a lipid-coated nanobubble and subsequent liposome formation. Sci. Rep. **2016**, 6, 28164. [CrossRef] [PubMed]

Kumar, B., Priyadarshi, R., Sauraj, Deeba, F., Kulshreshtha, A., Gaikwad, K. K., Kim, J., Kumar, A., & Negi, Y. S. (2020). Nanoporous Sodium Carboxymethyl Cellulose-*g*-poly (Sodium Acrylate)/$FeCl_3$ Hydrogel Beads: Synthesis and Characterization. *Gels (Basel, Switzerland)*, *6*(4), 49. https://doi.org/10.3390/gels6040049

Kumar, V.; Gabrilovich, D.I. Hypoxia-inducible factors in regulation of immune responses in tumour microenvironment. Immunology **2014**, 143, 512–519. [CrossRef] [PubMed]
L. R. Sayadi, D. A. Banyard, M. E. Ziegler, Z. Obagi, J. Prussak, M. J. Klopfer, et al., Topical oxygen therapy & micro/nanobubbles: a new modality for tissue oxygen delivery, Int. Wound J., 2018, 15(3), 363–374.

Larue, L.; Myrzakhmetov, B.; Ben-Mihoub, A.; Moussaron, A.; Thomas, N.; Arnoux, P.; Baros, F.; Vanderesse, R.; Acherar, S.; Frochot, C. Fighting hypoxia to improve PDT. Pharmaceuticals **2019**, 12, 115. [CrossRef]

Lee, M.; Lee, E.Y.; Lee, D.; Park, B.J. Stabilization and fabrication of microbubbles: Applications for medical purposes and functional materials. Soft Matter **2015**, 11, 2067–2079. [CrossRef] [PubMed]

Legband, N.D.; Feshitan, J.A.; Borden, M.A.; Terry, B.S. Evaluation of peritoneal microbubble oxygenation therapy in a rabbit model of hypoxemia. Trans. Biomed. Eng. **2015**, 62, 1376–1382. [CrossRef] [PubMed]

Levkovsky, A., Dardik, R., Barazany, D., Steinberg, D. M., Kirichenko, M. D., Apter, S., Peleg, E., Silverberg, D., Grossman, E., & Salomon, O. (2020). The effect of civil and military flights on coagulation, fibrinolysis and blood flow: insight from a rat model. *Thrombosis journal*, *18*, 24. https://doi.org/10.1186/s12959-020-00237-8

Lewis, P., & O'Halloran, K. D. (2016). Diaphragm Muscle Adaptation to Sustained Hypoxia: Lessons from Animal Models with Relevance to High Altitude and Chronic Respiratory Diseases. *Frontiers in physiology*, *7*, 623. https://doi.org/10.3389/fphys.2016.00623

Li, B.; Wen, H.M.; Cui, Y.J.; Zhou, W.; Qian, G.D.; Chen, B.L. Emerging multifunctional metal-organic framework materials. Adv. Mater. **2016**, 28, 8819–8860. [CrossRef] [PubMed]

Li, J.; Wang, X.; Zhang, T.; Wang, C.; Huang, Z.; Luo, X.; Deng, Y. A review on phospholipids and their main applications in drug delivery systems. Asian J. Pharm. Sci. **2015**, 10, 81–98. [CrossRef]

Li, X.S.; Kwon, N.; Guo, T.; Liu, Z.; Yoon, J. Innovative strategies for hypoxic-tumor photodynamic therapy. Angew. Chem. Int. Edit. **2018**, 57, 11522–11531. [CrossRef] [PubMed]

Liu, K., Scott, J. B., Jing, G., & Li, J. (2021). Management of Postoperative Hypoxemia. *Respiratory care*, *66*(7), 1136–1149. https://doi.org/10.4187/respcare.08929
M. Kuriakose and M. A. Borden, Microbubbles and Nanodrops for photoacoustic tomography, Colloid Interface Sci., 2021, 101464.

Maclntyre N. R. (2014). Tissue hypoxia: implications for the respiratory clinician. *Respiratory care*, *59*(10), 1590–1596. https://doi.org/10.4187/respcare.03357

Mairba¨url H, Weber RE. Oxygen transport by hemoglobin. Compr Physiol 2012;2(2):1463-1489.

Mallat, J., Rahman, N., Hamed, F., Hernandez, G., & Fischer, M. O. (2022). Pathophysiology, mechanisms, and managements of tissue hypoxia. *Anaesthesia, critical care & pain medicine*, *41*(4), 101087. https://doi.org/10.1016/j.accpm.2022.101087

Manninen, Pirjo H.; Unger, Zoe M. (2016). "Hypoxia". In Prabhakar, Hemanshu (ed.). *Complications in Neuroanesthesia*. Academic Press (Elsevier). doi:10.1016/C2015-0-00811-5. ISBN 978-0-12-804075-1.

Martin, K.H.; Dayton, P.A. Current status and prospects for microbubbles in ultrasound theranostics. Wiley Interdiscip. Rev. Nanomed. Nanobiotechnol. **2013**, 5, 329–345. [CrossRef] [PubMed]

Matsuki, N.; Ichiba, S.; Ishikawa, T.; Nagano, O.; Takeda, M.; Ujike, Y.; Yamaguchi, T. Blood oxygenation using microbubble suspensions. Eur. Biophys. J. **2012**, 41, 571–578. [CrossRef] [PubMed]

Mayeen, A., Shaji, L. K., Nair, A. K., & Kalarikkal, N. (2018). Morphological Characterization of Nanomaterials. In Elsevier eBooks (pp. 335–364). https://doi.org/10.1016/b978-0-08-101973-3.00012-2

Mc Ewan, C., Fowley, C., McHale, A. P., Atchison, J., Nomikou, N., & Callan, J. F. (2015). Treating cancer with sonodynamic therapy: a review. *International Journal of Hyperthermia*, *31*(2), 107-117.

Meegoda, J. N., Hewage, S and Batago, J, H. (2018) Stablity of Nanobubbles, Environmental Engineering Science

Mikalsen IB, Davis P, Øymar K. High flow nasal cannula in children: a literature review. Scand J Trauma Resusc Emerg Med. (2016) 24:93. doi: 10.1186/s13049-016-0278-4

Mochalov, K.E., Solovyeva, D.O., Vaskan, I.S. *et al.* Scanning Near-Field Optical Nanospectrophotometry: a New Method for Nanoscale Measurements of the Absorption Spectra of Single Nanoobjects. *Tech. Phys. Lett.* **45**, 138–141 (2019). https://doi.org/10.1134/S1063785019020287

N. N. Zhang, W. Lu, X. J. Cheng, J. Y. Liu, Y. H. Zhou and F. Li, High-powered microwave ablation of larger hepatocellular carcinoma: evaluation of recurrence rate and factors related to recurrence, Clin. Radiol., 2015, 70(11), 1237–1243.

Ninivaggi, M., de Laat, M., Lancé, M. M., Kicken, C. H., Pelkmans, L., Bloemen, S., Dirks, M. L., van Loon, L. J., Govers-Riemslag, J. W., Lindhout, T., Konings, J., & de Laat, B. (2015). Hypoxia Induces a Prothrombotic State Independently of the Physical Activity. *PloS one*, *10*(10), e0141797. https://doi.org/10.1371/journal.pone.0141797

Nolasco, S., Manti, S., Leonardi, S., Vancheri, C., & Spicuzza, L. (2022). High-Flow Nasal Cannula Oxygen Therapy: Physiological Mechanisms and Clinical Applications in Children. *Frontiers in medicine*, *9*, 920549. https://doi.org/10.3389/fmed.2022.920549

Nyankima AG, Rojas JD, Cianciolo R, Johnson KA, Dayton PA (2018) In vivo assessment of the potential for renal bio-efects from the vaporization of perfuorocarbon phase-change contrast agents. Ultrasound Med Biol 44:368–376

Othman, N. (2022b). IR Spectroscopy in Qualitative and Quantitative Analysis. In IntechOpen eBooks. https://doi.org/10.5772/intechopen.106625

Owen, J.; McEwan, C.; Nesbitt, H.; Bovornchutichai, P.; Averre, R.; Borden, M.; McHale, A.P.; Callan, J.F.; Stride, E. Reducing tumour hypoxia via oral administration of oxygen nanobubbles. PLoS ONE **2016**, 11, e0168088. [CrossRef] [PubMed]
Pawlowski, M.C.L.; Tian, L.L.; Pan, V.; Sen Gupta, A. Synthetic approaches to RBC mimicry and oxygen carrier systems. Biomacromolecules **2013**, 14, 939–948. [CrossRef]

Petersson, J., & Glenny, R. W. (2014). Gas exchange and ventilation-perfusion relationships in the lung. *The European respiratory journal*, *44*(4), 1023–1041. https://doi.org/10.1183/09031936.00037014

Pinto VL, Sharma S. Continuous Positive Airway Pressure. [Updated 2022 Jul 25]. In: StatPearls [Internet]. Treasure Island (FL): StatPearls

Pittman RN. Regulation of Tissue Oxygenation. San Rafael (CA): Morgan & Claypool Life Sciences; 2011.

Pugh C. W. (2016). Modulation of the Hypoxic Response. *Advances in experimental medicine and biology*, *903*, 259–271. https://doi.org/10.1007/978-1-4899-7678-9_18

R. H. Perera, A. D. Leon, X. Wang, Y. Wang, P. Peiris, E. Abenojar, et al., Real time ultrasound molecular imaging of prostate cancer with PSMA-targeted nanobubbles, Nanomed. Nanotechnol. Biol. Med., 2020, 28, 102213.

R. H. Perera, L. Solorio, H. Wu, M. Gangolli, E. Silverman, C. Hernandez, et al., Nanobubble ultrasound contrast agents for enhanced delivery of thermal sensitizer to tumors undergoing radiofrequency ablation, Pharm. Res., 2013, 31(6), 1407–1417.

R. Suzuki, Y. Oda, D. Omata, N. Nishiie, R. Koshima, Y. Shiono, et al., Tumor growth suppression by the combination of nanobubbles and ultrasound, Cancer Sci.,2016, 107(3), 217–223.

R. Suzuki, Y. Oda, N. Utoguchi and K. Maruyama, Progress in the development of ultrasound-mediated gene delivery systems utilizing nano- and microbubbles, J. Control. Release, 2011, 149(1), 36–41.

Rojas JD, Dayton PA (2019) In vivo molecular imaging using lowboiling-point phase-change contrast agents: a proof-of-concept study. Ultrasound Med Biol 45:177–191
S. Arakawa, M. Sugisawa and A. Leewananthawet, Application of Ozone Nanobubble Water (ONBW) to Peri-Implantitis Treatment, Dentistry, 2017, 7(12), 1–6.

Salama, H. E., Abdel Aziz, M. S., & Alsehli, M. (2019). Carboxymethyl cellulose/sodium alginate/chitosan biguanidine hydrochloride ternary system for edible coatings. *International journal of biological macromolecules*, *139*, 614–620. https://doi.org/10.1016/j.ijbiomac.2019.08.008

Sánchez-Baracaldo, P., & Cardona, T. (2020). On the origin of oxygenic photosynthesis and

Scimeca, M., Bischetti, S., Lamsira, H. K., Bonfiglio, R., & Bonanno, E. (2018). Energy Dispersive X-ray (EDX) microanalysis: A powerful tool in biomedical research and diagnosis. European journal of histochemistry: EJH, 62(1), 2841. https://doi.org/10.4081/ejh.2018.2841

Semenza GL. Hypoxia inducible factors in physiology and medicine. Cell 2012;148(3):399-408.

Sheriff, A., Kayser, S., Brunner, P., & Vogt, B. (2021). C-Reactive Protein Triggers Cell Death in Ischemic Cells. *Frontiers in immunology*, *12*, 630430. https://doi.org/10.3389/fimmu.2021.630430

Shih, C. Y., Wang, P. T., Su, W. C., Teng, H., & Huang, W. L. (2021). Nanomedicine-Based Strategies Assisting Photodynamic Therapy for Hypoxic Tumors: State-of-the-Art Approaches and Emerging Trends. *Biomedicines*, *9*(2), 137. https://doi.org/10.3390/biomedicines9020137

Song, R.Y.; Hu, D.H.; Chung, H.Y.; Sheng, Z.H.; Yao, S.H. Lipid-polymer bilaminar oxygen nanobubbles for enhanced photodynamic therapy of cancer. ACS Appl. Mater. Interfaces **2018**, 10, 36805–36813. [CrossRef] [PubMed]

Song, R.Y.; Peng, S.; Lin, Q.G.; Luo, M.; Chung, H.Y.; Zhang, Y.L.; Yao, S.H. pH-responsive oxygen nanobubbles for spontaneous oxygen delivery in hypoxic tumors. Langmuir **2019**, 35, 10166–10172. [CrossRef]

Stirbet, A., Lazár, D., Guo, Y., & Govindjee, G. (2020). Photosynthesis: basics, history and modelling. *Annals of botany*, *126*(4), 511–537. https://doi.org/10.1093/aob/mcz171

Stride, E., & Edirisinghe, M. (2008). Novel microbubble preparation technologies. Soft Matter, 4(12), 2350. https://doi.org/10.1039/b809517p

Sun, Y.X.; Zhao, D.Y.; Wang, G.; Wang, Y.; Cao, L.L.; Sun, J.; Jiang, Q.K.; He, Z.G. Recent progress of hypoxia-modulated multifunctional nanomedicines to enhance photodynamic therapy: Opportunities, challenges, and future development. Acta Pharm. Sin. B **2020**, 10, 1382–1396. [CrossRef]

Thomas, L, M, D. (1998), Cinical Labaroty diagnonstics, 1st edition, TH – Books Verlagedellschaft mbH, Frankfurt

Upadhyay, A.; Dalvi, S.V.; Gupta, G.; Khanna, N. Effect of pegylation on performance of protein microbubbles and its comparison with lipid microbubbles. Mater. Sci. Eng. C **2017**, 71, 425–430. [CrossRef] [PubMed]

Ushikubo, F. Y., Furukawa, T., Nakagawa, R., Enari, M., Makino, Y., Kawagoe, Y., Shiina, T., & Oshita, S. (2010). Evidence of the existence and the stability of nano-bubbles in water. Colloids and Surfaces A: Physicochemical and Engineering Aspects, 361(1–3), 31–37. https://doi.org/10.1016/j.colsurfa.2010.03.005

Varney, J. A., Dong, V. S., Tsao, T., Sabir, M. S., Rivera, A. T., Ghula, S., Moriles, K. E., Cherukuri, M. L., Fazal, R., Azevedo, C. B., Mohamed, R. M., Jackson, G. R., Fleming, S. E., Rochez, D. E., Abbas, K. S., Shah, J. H., Minh, L. H. N., Osman, F., Rafla, S. M., & Huy, N. T. (2022). COVID-19 and arrhythmia: An overview. *Journal of cardiology*, *79*(4), 468–475. https://doi.org/10.1016/j.jjcc.2021.11.019

Viseu, A. (2020, September 23). nanomedicine. Encyclopedia Britannica. https://www.britannica.com/science/nanomedicine

W. Cui, S. Tavri, M. J. Benchimol, M. Itani, E. S. Olson, H. Zhang, et al., Biomaterials neural progenitor cells labeling with microbubble contrast agent for ultrasound imaging in vivo, Biomaterials, 2013, 34(21), 4926–4935.

Wang T, Chen R, Liu C, et al. Attention should be paid to venous thromboembolism prophylaxis in the management of COVID19. Lancet Haematol 2020;7(5):e362-3, https://doi. org/10.1016/S2352-3026(20)30109-5.

Wanigarathna, D.K.J.A.; Gao, J.; Liu, B. Metal organic frameworks for adsorption-based separation of fluorocompounds: A review. Mater. Adv. **2020**, 1, 310–320. [CrossRef]

Wei, Y., Jiao, Y., An, D., Li, D., Li, W., & Wei, Q. (2019). Review of Dissolved Oxygen Detection Technology: From Laboratory Analysis to Online Intelligent Detection. Sensors (Basel, Switzerland), 19(18), 3995. https://doi.org/10.3390/s19183995

Willhite, C. C., Karyakina, N. A., Yokel, R. A., Yenugadhati, N., Wisniewski, T. M., Arnold, I. M., Momoli, F., & Krewski, D. (2014). Systematic review of potential health risks posed by pharmaceutical, occupational and consumer exposures to metallic and nanoscale aluminum, aluminum oxides, aluminum hydroxide and its soluble salts. *Critical reviews in toxicology*, *44 Suppl 4*(Suppl 4), 1–80. https://doi.org/10.3109/10408444.2014.934439

Wilson, K.E.;Wang, T.Y.;Willmann, J.K. Acoustic and photoacoustic molecular imaging of cancer. J. Nucl. Med. **2013**, 54, 1851. [CrossRef] [PubMed]

Wu, H.; Rognin, N.G.; Krupka, T.M.; Solorio, L.; Yoshiara, H.; Guenette, G.; Sanders, C.; Kamiyama, N.; Exner, A.A. Acoustic characterization and pharmacokinetic analyses of new nanobubble ultrasound contrast agents. Ultrasound Med. Biol. **2013**, 39, 2137–2146. [CrossRef]

X. Zhang, Y. Zheng, Z. Wang, S. Huang, Y. Chen, W. Jiang, et al., Methotrexate-loaded PLGA nanobubbles for ultrasound imaging and synergistic targeted therapy of residual tumor during HIFU ablation, Biomaterials, 2014, 35(19), 5148–5161.

Xie Y, Wang J, Wang Z, Krug KA, Rinehart JD (2018) Perfuorocarbon-loaded polydopamine nanoparticles as ultrasound contrast agents. Nanoscale 10:12813–12819

Xiong, R., Xu, R. X., Huang, C., De Smedt, S., & Braeckmans, K. (2021). Stimuli-responsive nanobubbles for biomedical applications. *Chemical Society reviews*, *50*(9), 5746–5776. https://doi.org/10.1039/c9cs00839j

Xu, R.X. Multifunctional microbubbles and nanobubbles for photoacoustic imaging. Contrast Media Mol. Imaging **2011**, 6, 401–411. [CrossRef] [PubMed]

Y. Cao, Y. Chen, T. Yu, Y. Guo, F. Liu, Y. Yao, et al., Drug release from phase-changeable nanodroplets triggered by Low-intensity focused ultrasound, Theranostics, 2018, 8(5), 1327.

Yeo E. J. (2019). Hypoxia and aging. *Experimental & molecular medicine*, *51*(6), 1–15. https://doi.org/10.1038/s12276-019-0233-3

Yin, T.;Wang, P.; Zheng, R.; Zheng, B.; Cheng, D.; Zhang, X.; Shuai, X. Nanobubbles for enhanced ultrasound imaging of tumors. Int. J. Nanomed. **2012**, 7, 895.

Yoon, Y.I.; Kwon, Y.-S.; Cho, H.-S.; Heo, S.-H.; Park, K.S.; Park, S.G.; Lee, S.-H.; Hwang, S.I.; Kim, Y.I.; Jae, H.J. Ultrasound-mediated gene and drug delivery using a microbubble-liposome particle system. Theranostics **2014**, 4, 1133. [CrossRef] [PubMed]

Z. Yu, M. Hu, Z. Li, D. Xu and L. Zhu, Anti-G250 nanobody functionalized nanobubbles targeting renal cell carcinoma cells for ultrasound molecular imaging, Nanotechnology, 2020, 31(20), 205101.

Zenewicz L. A. (2017). Oxygen Levels and Immunological Studies. *Frontiers in immunology*, *8*, 324. https://doi.org/10.3389/fimmu.2017.00324

Zhang C, Cao H, Li Q *et al.* Enhancement effect of ultrasound-induced microbubble cavitation on branched polyethylenimine-mediated VEGF165 transfection with varied N/P ratio. *Ultrasound Med. Biol.* 39, 161–171 (2013).
Zhang, C.; Qin, W.-J.; Bai, X.-F.; Zhang, X.-Z. Nanomaterials to relieve tumor hypoxia for enhanced photodynamic therapy. Nano Today **2020**, 35, 100960. [CrossRef]

Zhang, J., Chen, Y., Deng, C., Zhang, L., Sun, Z., Wang, J., Yang, Y., Lv, Q., Han, W., & Xie, M. (2019). The Optimized Fabrication of a Novel Nanobubble for Tumor Imaging. *Frontiers in pharmacology*, *10*, 610. https://doi.org/10.3389/fphar.2019.00610

Zhang, J., Wei, L., & Zhao, Y. (2020). Synthesis of nanobubbles for improved ultrasound tumor-imaging applications. *3 Biotech*, *10*(1), 12. https://doi.org/10.1007/s13205-019-1992-1

Zhang, X., Zhang, R., Liu, H., Gao, H., & Liang, Z. (2018). Evaluating CO2 desorption performance in CO2-loaded aqueous tri-solvent blend amines with and without solid acid catalysts. *Applied energy*, *218*, 417-429.

Zhao, W.; Hu, X.; Duan, J.; Liu, T.; Liu, M.; Dong, Y. Oxygen release from nanobubbles adsorbed on hydrophobic particles. Chem. Phys. Lett. **2014**, 608, 224–228. [CrossRef]

Zhou, M.; Cavalieri, F.; Caruso, F.; Ashokkumar, M. Confinement of acoustic cavitation for the synthesis of protein-shelled nanobubbles for diagnostics and nucleic acid delivery. ACS Macro Lett. **2012**, 1, 853–856. [CrossRef]

Appendix I

Synthesis of Oxygen Nanobubbles

(Khan *et al*., 2019)

Principle

The application of sonic waves to the bulk material of sodium carboxymethyl cellulose (SCMC) leads to its break up into nano sized bubbles. When the intensity of an ultrasonic wave exceeds the cavitation threshold, tiny nuclei like structures form internally with varying actions in the opposite/negative pressure zone which leads the nuclei to shrink or dilate. If the nuclei like structures dilate to a certain magnitude, gas molecules dispersed in the solution transfer into the nucleus and develop into a nanobubble.

Materials required

1) 1% w/v Sodium carboxymethyl cellulose solution
2) 0.5M Phosphate buffered saline
3) Double distilled water
4) Oxygen gas
5) Membrane filter
6) 70% ethanol

Procedure

Three different concentrations of SCMC were prepared from 1% SCMC medical grade solution. 0.5 M phosphate buffered saline (PBS) was mixed with SCMC solution, to a final concentration of 0.25%, 0.5% and 0.75% SCMC in 0.1 M PBS. Oxygen gas was flushed into the solution through an inlet during the entire sonication process. This mixture was sonicated using a bathtub sonicator / probe tip sonicator at 130 Watt and 20 kHz for various durations like 5, 10, 15, 20 and 30 minutes (Khan *et al.*, 2019).

Appendix II

Particle Size Analysis

(Maguire *et al.*, 2018)

Principle

The principle of particle size analyzer is to determine the size of the particle based on scattering of a laser beam. The size of the particle is determined when the particle is in Brownian motion and the laser beam hits on the particle. The reflection of the laser beam after it hits the nanoparticle is used to calculate the size of the nanoparticle.

Procedure

The sample was filled in the sample cell. The laser beam passes through the attenuator and falls on the sample present in the sample cell which is in Brownian motion. There are two detectors at different angles like 90º and 173º. The diffracted laser beam is detected by the detectors and processed by the correlator. The correlator is connected to a computer which displays the measurement of the diameter and dispersion state of the nanobubbles. After measurement, the sample was disposed of or cleaned out of the cell.

Appendix III

Zeta Potential

(Aljamali, 2015)

Principle

Many nanoparticles or colloidal particles have a surface charge when they are in suspension. The particle velocity is then determined by measuring the Doppler shift in the scattered light. The particle velocity is proportional to the zeta potential, which is the electrical potential of the particle at the shear plane. As a result, this optical measurement of particle motion in the presence of an applied field may be utilized to calculate zeta potential.

Procedure

An electrokinetic analyzer with an adjustable gap cell was used to measure the zeta potential. The sample was filled in the sample well and placed in the analyzer. The surface zeta potential in a 0.001 M KCl electrolyte solution was measured as a function of pH by altering the

solution pH with the addition of 0.05M HCl or 0.05M NaOH using the instrument's programmed titration unit.

Appendix IV

Dissolved Oxygen Content

(Wei *et al*., 2019)

Principle

In an electrochemical oxygen sensor, dissolved oxygen diffuses from the sample through an oxygen permeable membrane into the sensor. This occurs when hydrogen peroxide helps in cleaving the polymer shell i.e., sodium carboxymethyl cellulose so that oxygen can be released from the nanobubble. An electrical signal is produced when oxygen reaches the sensor and undergoes a chemical reduction process.

Reagents

1) 30% w/v H_2O_2
2) Deoxygenated Phosphate buffered saline pH 7.4
3) 0.1 N sodium hydroxide
4) 37 % Hydrochloric acid

Procedure

A dissolved oxygen meter was used to calculate the amount of O_2 produced by sodium carboxy methyl cellulose oxygen nanobubbles. For this, a rubber stopper is used to seal the dissolved oxygen meter probe, which has been submerged to almost the bottom of the flask. The flask was injected with 100 mL of deoxygenated 0.1 M PBS (pH 6.5) or 0.1 M PBS (pH 7.4). Then, to produce the H_2O_2 solution with a concentration of 100 μM, 2 μl of 30% w/v H_2O_2 was introduced into the flask. After the reading from the detector stabilized, the sodium carboxymethyl cellulose oxygen nanobubbles solution was introduced into the flask. Throughout the experiment, the flask was gently shaken. At predefined periods, the levels of the dissolved O_2 measured by the probe were recorded.

Appendix V

Field Emission Scanning Electron Microscopy - Energy Dispersive X-Ray

(Khan *et al.*, 2019)

Principle

SEM is a type of electron microscopy which is based on a focused beam of electrons that scans the sample. The electrons are liberated from a field emission source and scan the object according to a zig zag pattern. These electrons interact with the atoms in the sample to provide the surface topography.

Procedure

The fresh sample was placed on a carbon conductive tape and sputtered with gold plasma at 30,000 volts current. The sputtering process aids in preventing charge build up on the sample surface while scanning the sample. Electrons produced from electron gun enter the sample surface and produce signals regarding the surface morphology of the sample. The sample and the electron beam exchange energy, which results in the production of electromagnetic radiation, secondary electrons, high-energy electrons and electromagnetic radiation, all of which may be detected by specialized detectors. The signals are amplified by electronic amplifiers and shown on a computer monitor as variations in brightness.

After sputtering with gold, the sample was taken under EDX analyzer. It generates data made up of spectra with peaks corresponding to the various components that are present in the sample.

Appendix VI

Fourier Transform Infrared Spectroscopy (FTIR)

(Othman, 2022)

Principle

Functional groups have different vibration frequencies. Each vibration frequency has a different characteristic of that functional group. All the different vibration frequencies are within the infrared (IR) frequency range. The passing of Infrared rays through the organic compound causes the functional groups to vibrate at specific frequencies. Interferograms are decoded into

identifiable spectra to produce an FTIR spectrum. The Fourier Transform produces spectra that can be used to identify or quantify the substance.

Procedure

The beam from an IR source pass through a monochromatic controller with a selector, ensuring that only specific wavelengths are emitted, which may vary from 4000 to 400 cm^{-1}. The sample is placed in a holder in the path of the infrared source. A detector reads the analog signal and converts the signal to a spectrum. A computer is used to analyze the signals and identify the peaks.

Appendix VII
Three-Dimensional Optical Profiler
(Kaplonek *et al*., 2020)

Principle

A 3D Optical Profiler is typically a microscope containing two pathways for a light source splitted by a beam splitter. One reaches the reference mirror and the other is directed to the test sample. Both the reflections are combined and projected on an array detector. The surface's topographic characteristics are translated into interference fringe signals and the surface's three-dimensional topography is determined by observing how the interference fringes vary.

Procedure

To analyze the surface area of sodium carboxymethyl cellulose oxygen nanobubbles, a LASER PROFILOMETER - Zeta-20 was used and the sample was put beneath the loading platform's lens. The maximum scanning range was found to be 37 mm in the confocal, focus variation optical methods. This 3D optical profiler has the ability to scan the particles of 2 nm range. The Senso SCAN 2.0 software provides the correct course of the measurement process and helps in the scanning of the sample. Senso MAP Premium software was used for advanced analysis and visualization of the surface microtopography.

Appendix VIII

Transmission Electron Microscopy

(Khan *et al.*, 2019)

Principle

Transmission electron microscopy (TEM) provides images obtained by a beam of electrons transmitted through a thin specimen, which allows the detailed visualization of the interior of the sample.

Procedure

Samples for TEM were prepared by negative staining using uranyl acetate. First, a copper grid was dipped in nanobubbles and dried. Then, it was washed and negatively stained with 2% uranyl acetate solution. These grids were then utilized for TEM imaging.

Appendix IX

C Reactive Protein Assay

(Thomas *et al*., 1998)

Principle

C Reactive protein determination is a turbidimetric immunoassay in blood serum and is based on the principle of agglutination reaction. The test specimen is mixed with activation buffer (R1) and antibody reagent (R2) is then allowed to react. Presence of CRP in the test specimen results in the formation of an insoluble complex producing a turbidity, which is measured at 340 nm wavelength. The increase in turbidity corresponds to the concentration of CRP in the test specimen.

Reagents

1) Activation Buffer
2) Anti CRP Reagent
3) Calibrator
4) Serum Sample

Procedure

The calibrator was reconstituted exactly with 1.0 ml of distilled water, waited for 10 minutes, gently swirled the vial till the solution obtained homogeneity. Diluted the calibrator serially, using saline, such that the concentration of the CRP calibrator ranges from 10 mg/dl to 0.6 mg/dl. The zero concentration in the curve was obtained by adding saline instead of calibrator.

Zeroed the instrument with distilled water. Pipetted 500 µl of activation buffer and 50 µl of diluted calibrator in the measuring cuvette. Mixed well and incubated for 5 minutes at 37˚C. Read absorbance (A1) at 340 nm. Added 50 µl of Anti CRP Reagent (preincubated) at 37˚C, mix gently and read absorbance (A2) at 340 nm, at the end of exactly 5 minutes. Repeated the steps for each diluted calibrator for preparing the curve. The sample readings were obtained by adding them in the place of the calibrator. Calculated the difference between the absorbance Δ (A2 – A1) for each calibrator to prepare the curve. Plotted a graph of ΔA versus concentration of CRP on the graph paper and extrapolated the concentration values for the sample.

Appendix X

Fibrinogen Assay

(Thomas *et al*., 1998)

Principle

Determination of fibrinogen is a turbidimetric assay and is based on the principle of agglutination reaction. The test specimen is mixed with antibody reagent (R2) and activation buffer (R1) and allowed to react. Presence of fibrinogen in the test specimen results in the formation of an insoluble complex resulting in an increase in turbidity, which is measured at wavelength 340 nm. The increase in turbidity corresponds to the concentration of fibrinogen in the test specimen.

Reagents

1) Activation Buffer
2) Anti-Fibrinogen Reagent
3) Calibrator
4) Plasma Sample

Procedure

The calibrator was reconstituted exactly with 1.0 ml of distilled water, waited for 10 minutes, gently swirled the vial till the solution obtained homogeneity. Diluted the calibrator serially, using saline, such that the concentration of the fibrinogen calibrator ranges from 50 mg/dl to 1.5 mg/dl. The zero concentration in the curve was obtained by adding saline instead of calibrator.

Zeroed the instrument with distilled water. Pipetted 500 µl of activation buffer and 20 µl of diluted calibrator in the measuring cuvette. Mixed well and incubated for 5 minutes at 37˚C. Read absorbance (A1) at 340 nm. Added 50 µl of Anti-Fibrinogen Reagent (pre incubated at 37˚ C), mixed gently and read absorbance (A2) at 340 nm, at the end of exactly 5 minutes. Repeated the steps for each diluted calibrator for preparing the curve. The sample readings were obtained by adding them in the place of the calibrator. Calculated the difference between the absorbance Δ (A2 – A1) for each calibrator for preparing the curve. Plotted a graph of ΔA versus concentration of fibrinogen on the graph paper and extrapolated the concentration values for the sample.

Appendix XI

D-Dimer Assay

(Hirsh *et al*., 1994)

Principle

Determination of D-Dimer is a turbidimetric assay and is based on the principle of agglutination reaction. The test specimen is mixed with latex reagent (R2) and activation buffer (R1) and allowed to react. Presence of D-Dimer in the test specimen results in the formation of an insoluble complex resulting in an increase in turbidity, which is measured at wavelength 630 nm. The increase in turbidity corresponds to the concentration of D-Dimer in the test specimen.

Reagents

1) Activation Buffer
2) D-Dimer Latex Reagent
3) Calibrator
4) Plasma Sample

Procedure

The calibrator was reconstituted exactly with 1.0 ml of distilled water, waited for 10 minutes, gently swirled the vial till the solution attains homogeneity. Diluted the calibrator serially, using saline, such that the concentration of the D-Dimer calibrator ranges from 400 ng/ml to 50 ng/ml. The zero concentration in the curve was obtained by adding saline instead of calibrator.

Zeroed the instrument with distilled water. Pipetted 400 µl of activation buffer and 100 µl of latex reagent, in the measuring cuvette. Mixed well and incubated for 5 minutes at 37˚C. Added 30 µl of diluted calibrator, mixed well and read absorbance (A1) exactly at 10 seconds at 630 nm. Read absorbance (A2) at the end of exactly 5 minutes at 630 nm. Repeated the steps for each diluted calibrator for preparing the curve. The sample readings were obtained by adding them in the place of the calibrator. Calculated the difference between the absorbance Δ (A2 – A1) for each calibrator for preparing the curve. Plotted a graph of ΔA versus concentration of D-Dimer on the graph paper and extrapolated the concentration values for the sample.